
Article:
Deng, W. orcid.org/0000-0002-1793-8455, Backhouse, D.J., Kazi, F.K. et al. (6 more authors) (2023) Alternative raw material research for decarbonisation of UK glass manufacture. International Journal of Applied Glass Science, 14 (3). pp. 341-365. ISSN 2041-1286

https://doi.org/10.1111/ijag.16637

Received: 14 October 2022 | Revised: 5 March 2023 | Accepted: 13 April 2023

DOI: 10.1111/ijag.16637

INTERNATIONAL JOURNAL OF Applied Glass SCIENCE

RESEARCH ARTICLE

Alternative raw material research for decarbonization of UK glass manufacture

Wei Deng[1] | **Daniel J. Backhouse**[1] | **Feroz Kabir Kazi**[1] | **Ronak Janani**[1] | **Chris Holcroft**[2] | **Marlin Magallanes**[2] | **Martyn Marshall**[2] | **Caroline M. Jackson**[3] | **Paul A. Bingham**[1]

[1]Materials and Engineering Research Institute, College of Business, Technology and Engineering, Sheffield Hallam University, Sheffield, UK

[2]Glass Technology Services Ltd, Sheffield, South Yorkshire, UK

[3]Department of Archaeology, University of Sheffield, Sheffield, UK

Correspondence
Wei Deng and Paul A. Bingham, Materials and Engineering Research Institute, Sheffield Hallam University, Sheffield S1 1WB, UK.
Email: wei.deng@shu.ac.uk and p.a.bingham@shu.ac.uk

Funding information
Innovate UK, Grant/Award Number: 49096; UKRI / EPSRC, Grant/Award Number: EP/V054627/1; NERC, Grant/Award Number: OSS/345/0507

Abstract

Based on the current UK decarbonization policy, a general outlook on potential routes for the glass industry to achieve net-zero is discussed and the differentiation during decarbonization is specified. Biomass ash is considered a potential alternative raw material for low-carbon glass manufacture as it is rich in certain advantageous components, chiefly network modifiers. Simple sieving processes were shown to effectively separate impurities such as S, Cl, and C from some biomass ashes according to particle size distribution. The concentration of undesirable impurities decreased with increasing particle size. Morphologies and X-ray diffraction patterns of larger washed biomass ash particles indicated liquid/amorphous phase formation during biomass combustion. The washing of ashes was also shown to be a potential route to purification. A washed bracken ash relevant to both modern and ancient glass production was characterized for comparison. Ultraviolet-visible near-infrared (UV-Vis-near IR) absorption spectra of representative green container glasses produced using biomass ash confirmed that ~5 wt.% ash in representative glass batches has little impact on the color and redox state of glasses; the redox status of glass produced using >2 mm biomass ash after washing was less reduced than that of glass produced using high levels (>~9 wt.%) of >2 mm biomass ash after sieving alone, observed via the redox couple Cr^{3+}/Cr^{6+} by UV-Vis-near IR absorption spectroscopy.

KEYWORDS
decarbonization, glass manufacturing, raw materials

1 | INTRODUCTION

1.1 | Prospects for decarbonization of the glass industry

Commercial glass manufacture is a critical sector that is also energy-intensive and a major source of carbon emissions.[1] The UK glass manufacturing industry is significant, with 10 companies operating across 17 sites. Over the past 40 years, the average energy efficiency of UK glass furnaces has increased by 50%.[1] In 2015, The Paris Agreement set a target to reduce greenhouse gas emissions by at least 40% by 2030 and 80% by 2050 compared to 1990 levels. Meanwhile, the UK Government and British Glass

published their Glass Decarbonization Roadmaps to 2050[2,3] to help coordinate and support the achievement of decarbonization goals within the glass sector. Both Roadmaps highlight glass batch reformulation as one enabler for the glass industry to reduce its energy consumption and CO_2 emissions. In 2021, the UK government committed to an even more ambitious target of net-zero greenhouse gas emissions by 2050,[4] which places enormous commitments on the so-called Foundation Industries that include the glass sector.

Michael et al.[5] reviewed the decarbonization options for the glass industry in 2021. According to their analysis, electricity and hydrogen will be likely future energy carriers; oxy-fuel combustion and waste heat recovery will be critical and applied more extensively. In 2022, Dylan et al.[6] gave a critical and systematic review of developments and sociotechnical systems for glass industry decarbonization; the study identified carbon-intensive processes in the glass industry and highlighted many barriers and promising avenues for future research. It also highlighted the current lack of consensus on the most promising technologies to achieve net zero in the glass industry.

The next 20–30 years will be critical for change and decarbonization before stable low-carbon energy carriers are implemented and become established. Glass batch raw materials, production processes, and furnace designs may undergo a transitional period with significant changes if the net-zero policy is implemented as planned. It is worth noting that glass is a typical mature capital-intensive industry. Investment costs for new technology development are enormous, and the risks are high.[1–6] It is an important step to set up non-profit organizations during this period to guide the development of new technologies, attract capital interest, reduce risk, and protect intellectual property rights.[7] Ideally, new melting designs/technologies and novel alternative batch compositions will continue to emerge and vary according to the capital and plant scale. Meanwhile, the plant position and local energy generation/supply will also have an impact on decarbonization routes. This pattern is already reflected in the most recent industrial activities. For example in the UK, NSG Pilkington successfully fired its St. Helens float glass furnace with a sustainable biofuel manufactured from organic waste materials,[8] in addition to the world's first successful hydrogen glass melting trial[9] and Encirc 360 with Glass Futures successfully fired a container glass furnace using biofuels and manufactured containers using 100% cullet.[10] In Spain, Vidrala is to construct a 12 MW solar photovoltaic power generation facility at its glass manufacturing site for substituting fossil and electrical energy from the grid.[11] In Germany, the ZeroCO_2-Glas consortium aims to develop CO_2-neutral container glass production, carbonate-free raw materials, a highly flexible hybrid tank furnace with electric and hydrogen firing, and a revolutionary submerged feeding approach.[12] O-I Glass, a multinational corporation, has secured a deal with Engie, which will supply renewable energy to its container glass manufacturing sites across Europe.[13] Similarly, Allied Glass also signed a deal with Drax for 100% renewable hydropower.[14] Comparison between these different technologies will be incredibly informative and valuable. Generally, these new technologies should include but are not limited to, reducing carbon emissions. However, they may also have other impacts such as reducing energy (fuel) consumption and/or reusing waste raw materials to provide cost-saving and greater sustainability. Regarding the glass production process, it is always critical to emphasize the stability and consistency of raw materials, fuels, temperatures, and hence, melting and forming characteristics of the glass. Alternative glass raw materials, fuel switching, supply condition variation, and hybrid combustion may challenge that stability. Applying new technologies to enhance the adaptability of the process to meet the comprehensive challenge, and identifying those stable nodes during supply chains and manufacturing processes will be primary future research directions. It is also important to highlight that energy-saving can improve efficiency and reduce CO_2 emissions since 58% of CO_2 emissions during glass manufacture arise from fossil fuel combustion.[2,3] This makes emissions reductions through energy conservation aligned with commercial interests to achieve optimal solutions, which should always be fully considered.

According to the Industrial Decarbonization and Energy Efficiency Roadmaps to 2050,[2,3] decarbonization is progressing in all Foundation Industries, as illustrated by recent significant UK government investments in Transforming Foundation Industries (TFI),[5,6] which includes the TFI TransFIRe Hub[15] and the TFI Network Plus.[16] These changes in the industrial environment also provide opportunities for the glass sector to explore new approaches and technologies, with the potential for symbiotic win-win relationships with other sectors. For example, the energy generation sector is switching fuel from coal to biomass to generate electricity in response to UK decarbonization policies.[17] Being renewable converts biomass into an essential fuel to be considered for sustainable development and the fight against climate change through fossil fuel CO_2 emissions reduction[4,17,18] One of the most important applications is the direct combustion of woody biomass in boilers for power generation.[19,20] Much of the resulting biomass ash is currently sent to landfills as waste.[20–24] However, a similar substance, plant ash, had historically been produced as a critical glassmaking raw material for thousands of years until relatively recently.[25]

1.2 | The historical basis of biomass ash as a glassmaking raw material

Ashes from the the combustion of plants and their derivatives, such as *potash*,[25] have been essential alkali sources for glassmakers throughout at least the last 3000 years.[26–30] In prehistory, the ashes of halophytic plants were used to fabricate glazed stones and faience.[31] Analyses of glazes on steatite and faience samples from the Middle Kingdom and Second Intermediate Periods in Egypt (2055–1550 BC) show high potash contents,[31,32] indicating that plant ash was the source of the alkali flux used.[33] According to archaeological records, significant quantities of glass produced from the Late Bronze Age, around 1500 BC, in the Near East, were of the plant ash type, with high MgO and K_2O contents[33] and relatively high concentrations of CaO which acted as a stabilizer, although there was some experimentation with trona as a raw material.[34] From the mid-first millennium BC, natron glasses became more common and natron became the major flux for glassmaking in the eastern Mediterranean and Levantine regions.[35] However, high-sodium plant ash continued to be used as a flux in the East such as in Mesopotamia, Iran, and Central Asia.[33] Natron glass was not made in small furnaces on a local level[35,36]; the initial production of glass from raw materials was a major industry that produced large quantities of "raw glass" at only a few key centers at this time.[36]

Plant ashes were sometimes added to glass batches to influence the glass color or to extend the supply of glassmaking raw materials. For example, in the early Roman Imperial period (1st Century AD),[37] there is evidence that emerald green Roman glasses were probably produced by adding plant-ash flux into a mineral soda natron glass, which was the more common type of glass in the Roman period. Similarly, in northern Europe from the 6th Century AD, recycled Roman glass also contained some wood ashes.[38] By the 10th Century AD glassmaking in parts of southern Europe had developed using soda-rich plant ashes from the Levant and Egypt, such as that produced in Venice,[38] whilst in Northern Europe ashes from woodland plants, for example, oak, beech, and ferns, were a source of the alkali flux which continued throughout the Middle Ages and into the early modern period. Glasses resulting from hardwood ashes are known as "forest glasses"[39] since they are rich in potassium and calcium arising from the wood ashes used as the major raw materials. These forest glasses required higher temperatures for melting, in the range of 1300°C, much higher than that needed to melt natron or soda-ash glass (around 1100°C).[36] Fern ashes were also used as a source of alkali flux for glassmaking throughout both northern and southern Europe as late as the 18th Century.[38,40,41] For example, glassmakers in the Alsace region used fern ashes among their raw materials to produce 'Verre de Fougere' (forest glass), and it is possible that in the 16th Century, purified fern ash was used in a number of northern glasshouses to imitate Cristallo, a fine, high-quality glass produced in Italy.[42]

To make clear, colorless, and high-quality glass, Biringuccio in his 16th Century Italian treatise described glass production using fern ashes which were washed, and the purified evaporate dried for use as salt.[43,44] However, in 1306, the official Venetian glassmakers' guild regulations forbade the use of fern ash as a flux because it was said to produce poor-quality glass.[45] For high-quality lead crystal glasses, the ash used needed to be purified[46] so lixiviating or leaching the ashes and using the evaporates may have been one solution.[46] Indeed, the word *potash* derives from a translation of the older Dutch word *potaschen*, literally "*pot ashes*", as potash was originally obtained by soaking wood ash in water and evaporating the mixture in an iron pot. In 1780, James King, a merchant from Newcastle-upon-Tyne patented his British Barilla,[47] which clearly documented the process to produce this potash from different plant ashes. In July 1790, the first US patent ever granted, number X000001, was issued to Samuel Hopkins for an improvement in "The making of Pot ash and Pearl ash using new Apparatus and Process",[48] by which pearl ash was a purer quality material made by the calcination of potash.

In 1787, Nicolas Leblanc prepared artificial-synthetic soda by 'the black ash process' for the first time.[25] However, the production of synthetic soda did not become economically viable until the late 19th Century and so the dependence on organic sources of potash persisted.[25] In 1823, James Muspratt built plants in the UK for the production of synthetic soda by the Leblanc method, and manufactured soda rapidly replacing the imported Barilla and ash from kelp or seaweed as the major source of alkali for good quality British glassmaking.[25] Since then, plant ash or its derivatives were gradually removed from commercial glass manufacture.[25,49] This integration did not come suddenly into being with the emergence of Leblanc's process, but took place hesitantly alongside anciently established procedures for extracting alkali from the ashes of land and maritime plants.[49] The emergence of a synthetic alkali industry in England was delayed until a stage was reached at which the limited harvests of natural alkali could no longer meet the requirements of the expanding soap and textile industries, and, more particularly, double-decomposition processes, based on American or Continental potash, could no longer cope with the chronic soda shortage.[49]

These historical processes relating to plant ashes are relevant today, in the 21st Century, as biomass ashes have become novel wastes since the fuels used in the UK energy sector have transformed or are transforming from coal or natural gas into renewable energy sources including biomass. Most ashes generated from biomass power plants are currently sent to landfill or used in lower-value applications such as road building, water, and soil treatment, or concrete and cement production after further processing.[20–24] However, the benefits of introducing biomass ash as an alternative glass raw material are potentially numerous.[50–52] It is therefore very important to note and understand the historical context of plant-based ashes in glassmaking. Biomass ashes are known to contain elements including Si, Al, Na, Mg, P, and especially K and Ca in the form of oxides, which have potential value in glass manufacture as alternative raw materials. During soda-lime-silica type container and flat glass production, which have by far the largest share of the UK and global glass markets, the decomposition of carbonate raw materials is responsible for 15%–25% of total CO_2 emissions.[4] Since most of the carbon in biomass has largely been combusted, biomass ash is thus a low-carbon by-product that could be a raw material for glass manufacture.[4]

In terms of scale, according to Ofgem's Biomass Sustainability report,[17] the total consumption of biomass by dedicated biomass facilities and cement kilns in the UK (excluding imports) was 5.8 MT in 2016–17. The UK has 226 biomass power plants fueled by recycled wood, virgin wood, straw and miscanthus, poultry litter, and sewage sludge. These plants generated 1.58 GWh or around 2.1% of the total UK power generation in 2020.[18]

1.3 | This work

After extensive investigations on different types of biomass ashes from multiple biomass power plants across the UK,[50,53] a typical bottom biomass ash, generated in a UK biomass power plant by burning herbaceous biomass fuel, was selected as a potential alternative raw material for glass manufacturing. Biomass ash samples were collected in different time periods during stable production phases for further processing and characterization. Here, three samples, S1 (collected on May 29, 2019), S2 (collected on December 5, 2019), and S3 (collected on May 15, 2019) were selected. Similarly to ancient glass manufacturing practices,[43,44] the as-received ashes were purified using sieving and washing in water. The chemical compositions of the ashes as a function of the particle size distribution after the sieving process were investigated using X-ray fluorescence (XRF) spectroscopy and LECO analysis. S1 was selected for further washing treatments due to its low carbon content. The crystalline phases, composition, and microstructure of different ash fractions after washing were investigated using X-ray diffraction (XRD), scanning electron microscopy (SEM), and energy-dispersive X-ray spectroscopy (EDX). Washed bracken salt and ash samples from previous research were also studied here for comparison and to represent ancient biomass batch additions.[42,54] For comparative glass melting and property assessments, a representative green container glass batch was melted as a benchmark. To highlight the impact on glass properties caused by the introduction of biomass, different amounts, ranging from 5 to 20 g, of biomass ashes after treatment were directly added into a 100 g green container glass batch,[55,56] and the batches were melted in laboratory conditions. The specific batch compositions are presented in Table 1. UV-Vis-IR absorption spectroscopy was utilized to determine the optical absorption spectra of those glasses, and hence the color and redox were characterized.

According to the 2008–2020 official statistics from the UK Department for Environment, Food, and Rural Affairs,[57] UK biomass power plants consumed a total of 0.97 Mt of herbaceous biomass fuel. Combustion of virgin herbaceous biomass produces 5–9 wt.% ash[58] and the annual yield of this biomass ash is approximately 48.5–87.3 kilotons. It is estimated that in 2019 approximately 0.66 Mt sodium carbonate was consumed by the UK glass sector, based on typical glass-making recipes.[4,59,60] We can thus infer that the UK container glass sector consumed ~0.4 Mt sodium carbonate per year.[4,59,60] If we consider only the potassium in biomass ash as a partial replacement for the sodium in sodium carbonate, theoretically, the biomass ash can save 56 000–98 000 tonnes of sodium carbonate in the UK container glass sector per year, which is up to 25% of its sodium carbonate consumption. In addition, based on these estimates, the partial replacement of sodium carbonate by biomass ash in glass batches could potentially save up to 64 000 tonnes of CO_2 emissions per year across the UK glass sector.[4]

2 | EXPERIMENTAL PROCEDURES

2.1 | Biomass ash treatment

2.1.1 | Sieving

After being collected from the UK biomass power plant, three batches of biomass bottom ash (S1, S2, and S3) generated in the same moving grate biomass power plant during stable production phases, were selected and placed in an electric oven for drying at 100°C for 24 h. The moisture weight loss at this stage was 1.5–2 wt.%. The ashes appeared as a black mixture of particles and clinkers, with diameters

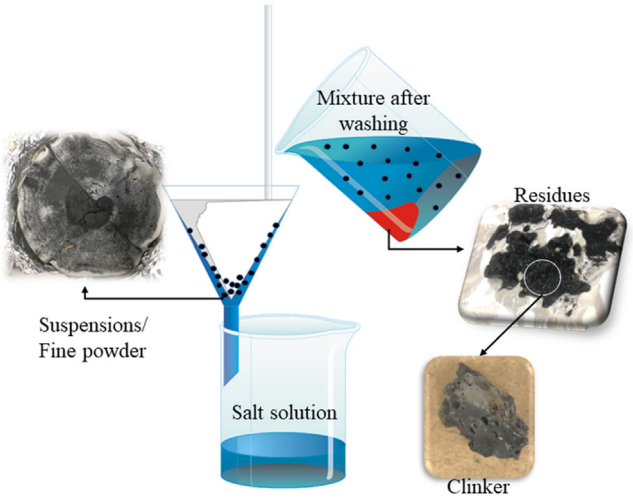

FIGURE 1 Schematic of the biomass ash filtration process used in this study, after washing the ash in deionized (DI) water at room temperature.

ranging from 4 cm to fine powders. The ashes were sieved through a metal sieve set (Fieldmaster). Two sieve mesh sizes, 10 (2000 μm) and 230 (63 μm), were selected to separate ashes into large, medium, and fine particle size fractions. To determine the chemical composition of each ash fraction, XRF and carbon LECO analyses were conducted.

2.1.2 | Washing and filtration

A washing and filtration process was applied to the S1 biomass ashes, as follows: 20 g of the dried as-received biomass ash was washed in 400 ml D.I. water (with a solid-to-liquid ratio of 1:40) in a beaker with a polymer-coated magnetic rotor spinning at 300 rpm for 40 min at room temperature. A mixture of solution with a fine, black suspension and settled ash residue was obtained. This mixture was then filtered through filter paper (F1/KA4, medium-fast; Smith, UK) at room temperature. The filtrate (filtered solution) was then placed in a beaker and evaporated in an electric oven at 90°C for 24 h until a dry salt layer formed in the beaker, which was then collected for XRD analysis. The filter cake (a fine solid material remaining on the filter paper) was also dried in air at 90°C for 24 h for SEM/EDX analysis. Similarly, the larger particles settled, and this washed ash residue was dried in an electric oven at 90°C for 24 h for further SEM/EDX study. In the residues, a black, visually vitreous-like clinker was observed. Figure 1 shows a schematic of the filtration process, and various fractions (filtrates, filter cake, and residues).

2.2 | Ancient bracken ash, salt, and insoluble residue preparation

Samples of bracken (Pteridium aquilinum L. Kuhn) ash and salt were provided by Jackson, Smedley et al.[42,43,54] from their previous ancient glass production process simulation research. Those bracken samples were collected at regular intervals throughout the spring, summer, and early autumn of 1999 from two geographically and ecologically different sites (Rugeley and Snake Pass) in Derbyshire, UK.[54] After being air-dried for six weeks, bracken samples were burned in a clean garden incinerator until ash was produced and the embers were cooled in order to simulate ancient glass raw material preparation practices. The highest temperatures recorded during combustion were more than 900°C.[54,61] The residue after burning was then collected for further re-ashing at 450°C for 30 mins to remove any remaining organic carbon.[61]

The salt and insoluble residue from bracken ash were prepared using the following procedure.[43] Two 500 g batches of bracken ash were each mixed for 30 min in 1 L of distilled water at room temperature. To remove the insoluble components the solution was filtered under vacuum. The procedure was then repeated on the insoluble products to extract any remaining soluble components and the solution evaporated to dryness. The resulting salts proved to be extremely deliquescent, readily absorbing atmospheric moisture, and so were stored at 80°C in a desiccator under vacuum.

2.3 | Glass preparation with biomass ash as a raw material

The representative (benchmark) green container glass batch[55,56] and modified batches containing biomass ashes were melted under laboratory conditions. As shown in Table 1A,B, different biomass ashes were added to the benchmark batch at several levels, from 4.76 to 16.67 wt.%. Batches were weighed to two decimal places to provide batches weighing 150 g. Batches were thoroughly mixed and were then placed in recrystallized Al_2O_3 crucibles. Crucibles were heated in an electric furnace at 4°C/min to 1450°C and then held at this temperature for 4 h. Crucibles were then removed from the furnace, and the molten glass was poured into a stainless steel mold and allowed to cool until sufficiently rigid to remove the mold. The glass was subsequently annealed in an electric furnace at 540°C for 1 h to remove thermal stresses and then cooled slowly to room temperature. The analyzed chemical compositions of the glasses produced are presented in Table 2.

TABLE 1a Batch compositions of Benchmark glass and glasses 1–12 containing different levels and pre-treatments of S1 biomass ash (in grams).

Ingredients (g)	Benchmark	1	2	3	4	5	6	7	8	9	10	11	12
Na_2CO_3	19.12	19.12	19.12	19.12	19.12	19.12	19.12	19.12	19.12	19.12	19.12	19.12	19.12
$MgCO_3$	3.69	3.69	3.69	3.69	3.69	3.69	3.69	3.69	3.69	3.69	3.69	3.69	3.69
SiO_2	58.33	58.33	58.33	58.33	58.33	58.33	58.33	58.33	58.33	58.33	58.33	58.33	58.33
$Al(OH)_3$	2.31	2.31	2.31	2.31	2.31	2.31	2.31	2.31	2.31	2.31	2.31	2.31	2.31
$CaCO_3$	15.17	15.17	15.17	15.17	15.17	15.17	15.17	15.17	15.17	15.17	15.17	15.17	15.17
K_2CO_3	0.84	0.84	0.84	0.84	0.84	0.84	0.84	0.84	0.84	0.84	0.84	0.84	0.84
Na_2SO_4	0.09	0.09	0.09	0.09	0.09	0.09	0.09	0.09	0.09	0.09	0.09	0.09	0.09
Fe_2O_3	0.28	0.28	0.28	0.28	0.28	0.28	0.28	0.28	0.28	0.28	0.28	0.28	0.28
Cr_2O_3	0.17	0.17	0.17	0.17	0.17	0.17	0.17	0.17	0.17	0.17	0.17	0.17	0.17
Suspension after washing		5.00											
Small particles (< 2 mm) after washing			5.00										
Large particles (> 2 mm) after washing				5.00				10.00	15.00	20.00			
<500 μm particles after sieving					5.00								
500 μm-2 mm particles after sieving						5.00							
>2 mm particles after sieving							5.00				10.00	15.00	20.00
SUM (g)	100.00	105.00	105.00	105.00	105.00	105.00	105.00	110.00	115.00	120.00	110.00	115.00	120.00

TABLE 1b Batch compositions of Benchmark glass and glasses 1–12 containing different levels and pre-treatments of S1 biomass ash (wt. %).

Ingredients	Benchmark	1	2	3	4	5	6	7	8	9	10	11	12
Na_2CO_3	19.12	18.21	18.21	18.21	18.21	18.21	18.21	17.38	16.63	15.94	17.38	16.63	15.94
$MgCO_3$	3.69	3.52	3.52	3.52	3.52	3.52	3.52	3.36	3.21	3.08	3.36	3.21	3.08
SiO_2	58.33	55.56	55.56	55.56	55.56	55.56	55.56	53.03	50.71	48.59	53.03	50.71	48.59
$Al(OH)_3$	2.31	2.20	2.20	2.20	2.20	2.20	2.20	2.10	2.01	1.93	2.10	2.01	1.93
$CaCO_3$	15.17	14.44	14.44	14.44	14.44	14.44	14.44	13.79	13.19	12.64	13.79	13.19	12.64
K_2CO_3	0.84	0.80	0.80	0.80	0.80	0.80	0.80	0.76	0.73	0.70	0.76	0.73	0.70
Na_2SO_4	0.09	0.08	0.08	0.08	0.08	0.08	0.08	0.08	0.08	0.07	0.08	0.08	0.07
Fe_2O_3	0.28	0.27	0.27	0.27	0.27	0.27	0.27	0.26	0.25	0.24	0.26	0.25	0.24
Cr_2O_3	0.17	0.16	0.16	0.16	0.16	0.16	0.16	0.15	0.15	0.14	0.15	0.15	0.14
Suspension after washing		4.76											
Small particles (< 2 mm) after washing			4.76										
Large particles (> 2 mm) after washing				4.76				9.09	13.04	16.67			
<500 μm particles after sieving					4.76								
500 μm-2 mm particles after sieving						4.76							
>2 mm particles after sieving							4.76				9.09	13.04	16.67
SUM (wt %)	100.00	100.00	100.00	100.00	100.00	100.00	100.00	100.00	100.00	100.00	100.00	100.00	100.00

TABLE 2 XRF analyses of Benchmark glass and glasses 1–12 containing different levels and pre-treatments of S1 biomass ash (wt. %).

Wt.%	Benchmark	1	2	3	4	5	6	7	8	9	10	11	12
Na_2O	13.926	12.304	13.196	13.525	13.350	13.117	13.109	11.385	11.780	11.327	12.575	11.171	11.302
MgO	1.508	1.364	1.486	1.534	1.500	1.477	1.520	1.302	1.475	1.474	1.572	1.344	1.423
Al_2O_3	1.697	1.441	1.617	1.665	1.589	1.699	1.761	1.404	1.450	1.443	1.748	1.401	1.438
SiO_2	66.763	68.472	67.234	66.998	67.493	66.841	67.100	65.914	67.104	67.482	66.592	66.352	67.106
SO_3	0.105	0.000	0.100	0.109	0.111	0.110	0.096	0.126	0.111	0.111	0.101	0.112	0.124
P_2O_5	0.000	0.072	0.091	0.076	0.077	0.071	0.070	0.122	0.186	0.222	0.129	0.199	0.216
Cl	0.042	0.040	0.000	0.045	0.000	0.000	0.050	0.000	0.000	0.000	0.000	0.051	0.060
K_2O	0.900	1.204	1.587	1.548	1.384	1.478	1.403	2.635	3.018	3.335	2.428	3.059	3.293
CaO	14.112	14.169	13.723	13.540	13.564	14.216	13.942	16.086	13.898	13.591	13.987	15.299	13.992
TiO_2	0.035	0.029	0.038	0.039	0.030	0.033	0.035	0.043	0.037	0.046	0.000	0.046	0.036
Cr_2O_3	0.308	0.309	0.292	0.291	0.298	0.302	0.295	0.327	0.269	0.262	0.263	0.307	0.270
Fe_2O_3	0.544	0.522	0.573	0.571	0.544	0.590	0.560	0.577	0.611	0.645	0.539	0.575	0.679
SrO	0.017	0.020	0.021	0.021	0.018	0.022	0.020	0.041	0.032	0.035	0.027	0.038	0.035
ZrO_2	0.043	0.054	0.042	0.038	0.042	0.044	0.039	0.038	0.029	0.027	0.039	0.046	0.026
SUM	100.00	100.00	100.00	100.00	100.00	100.00	100.00	100.00	100.00	100.00	100.00	100.00	100.00

2.4 | Characterisation and testing methods

Chemical compositions were determined using XRF spectroscopy (wavelength-dispersive Philips PW2440 sequential XRF spectrometer). Uncertainties associated with the XRF analysis are estimated at ±2 % of the measured concentrations. The XRF data were analyzed using a modified version of the OXI program.[62]

A total carbon elemental assay was conducted using a LECO CS844ES combustion furnace. The analysis was carried out by an ISO 17025 (UKAS) accredited testing facility, and the instrument was calibrated using appropriate certified reference materials.

Selected ash samples were characterized using XRD at room temperature, with a diffractometer (model: Empyrean XRD, PANalytical, Almelo, The Netherlands) equipped with a Cu tube operated at 40 kV, 40 mA, and 2θ ranging between 5 and 90° (0.016° increment per step). All samples were analyzed using a reflection spinner sample holder spinning at 0.25 Hz. All samples were pulverized to fine powders using a mortar and pestle prior to measurement.

To characterize the morphology, microstructure and composition distribution of ash samples, samples were coated with carbon (≈20 nm) for SEM (FEI Quanta 650) and EDX (Oxford 148 Instruments/point and mapping scan mode) characterization.

Glass samples were prepared for optical spectroscopy measurement by grinding using successively finer SiC grinding pads from 60 to 1200 grit size, then polished using a suspension of CeO_2 powder in water to provide a highly polished (<1 μm) surface finish. Optical absorption spectra were collected using a Shimadzu UV-3600Plus Series ultraviolet-visible near-infrared (UV-Vis-Near IR) spectrophotometer over the wavelength range of 190–2500 nm.

Based on the chemical compositions of glass samples, key viscosity points including melting point, working point, softening point, and annealing point, were modeled using the Lakatos model[63] and are listed in Table 3. The relative machine speed (RMS), working range index (WRI), and devitrification index[1,64] were also calculated for each glass formulation (Table 3). RMS is a widely used term in glass manufacturing and is defined as the relative average speed at which articles can be produced using a particular glass composition. Compositional changes have previously been used to modify RMS:[1,64]

$$\mathrm{RMS} = \frac{\mathrm{S} - 450}{(\mathrm{S} - \mathrm{A}) + 80}$$

where S = softening point /°C, defined as log (η / dPa.s) = 7.65 and A = Annealing Point /°C, defined as log (η / dPa s) = 13.0. (η is melt viscosity in dPa·s) WRI is defined as the temperature difference between the softening point (S) and the annealing point (A). WRI is used as an indicator of the working range and should not be confused with the actual working range. For most commercial soda-lime-silica container glasses, WRI > 160°C:[1,65]

$$\mathrm{WRI} = (\mathrm{S} - \mathrm{A})$$

The devitrification index (D) has previously been used to estimate the likelihood of devitrification problems.[1,64,65] A positive value for D indicates relative freedom from devitrification while a negative value indicates an increased

TABLE 3 Results from viscosity modeling and characterization of glasses (viscosity in dPa•s).

		Benchmark	1	2	3	4	5	6	7	8	9	10	11	12
Viscosity (°C) calculated by Lakatos[63] model	TLog2	1328	1367	1345	1340	1348	1337	1345	1320	1353	1366	1344	1336	1356
	TLog3	1096	1132	1109	1104	1111	1106	1112	1105	1120	1130	1112	1115	1124
	TLog4	965	993	975	971	977	973	977	973	984	991	978	980	987
	TLog6	777	797	784	780	783	784	786	791	792	798	786	795	797
	TLog7.6	718	737	722	718	722	723	725	736	729	732	725	736	732
	TLog13	557	565	557	554	557	559	559	566	558	558	558	564	559
Relative Machine Speed		1.111	1.141	1.109	1.101	1.108	1.118	1.120	1.145	1.111	1.112	1.114	1.134	1.114
Working Range Index (°C)		161	172	165	163	165	164	165	170	171	174	167	172	173
Devitrification Index (°C)		0.9	11.8	5.2	3.3	5.2	4.5	5.2	9.7	11.1	13.9	6.7	11.9	12.9

TABLE 4 Sieved biomass ashes fractions—Chemical composition analysis by XRF and LECO (wt.%).

Ash	S1				S2				S3			
Size (μm)	>2000	2000-63	<63	Total	>2000	2000-63	<63	Total	>2000	2000-63	<63	Total
Wt %	67%	17%	16%	100%[†]	72%	9%	19%	100%[†]	82%	9%	9%	100%[†]
Na_2O	0.61	0.65	1.37	0.74	0.00	0.44	0.92	0.23	0.47	0.49	0.65	0.50
MgO	1.65	1.91	1.28	1.63	1.45	1.66	1.61	1.51	1.53	1.30	1.12	1.48
Al_2O_3	3.43	1.17	0.95	2.64	0.83	1.24	0.98	0.90	1.29	1.52	0.93	1.28
SiO_2	59.32	74.29	75.91	64.61	71.23	61.06	52.01	66.47	59.54	44.18	41.56	56.38
P_2O_5	0.90	0.78	1.28	0.94	0.76	0.85	1.21	0.86	0.86	0.79	0.95	0.87
SO_3	0.44	0.25	0.59	0.43	0.15	0.49	1.14	0.39	0.27	0.52	1.14	0.40
K_2O	22.79	12.98	11.07	19.19	18.96	23.96	20.90	19.88	26.08	24.05	20.04	25.39
CaO	8.26	5.69	5.36	7.35	5.70	6.86	6.32	5.96	7.82	7.43	5.60	7.59
TiO_2	0.11	0.00	0.00	0.08	0.00	0.09	0.06	0.02	0.08	0.06	0.08	0.08
Fe_2O_3	1.93	0.59	0.45	1.46	0.35	0.48	0.46	0.38	0.81	0.65	0.53	0.77
SrO	0.04	0.03	0.00	0.03	0.03	0.03	0.03	0.03	0.04	0.03	0.03	0.04
Cl	0.29	0.43	0.53	0.35	0.11	0.44	1.08	0.35	0.43	0.65	1.33	0.56
BaO	0.00	0.00	0.00	0.00	0.00	0.00	0.00	0.00	0.00	0.11	0.00	0.01
MnO	0.00	0.00	0.00	0.00	0.00	0.00	0.00	0.00	0.23	0.00	0.00	0.18
C	0.23	1.22	1.22	0.56	0.43	2.41	13.30	3.02	0.55	18.21	26.05	4.46
SUM	100.00	100.00	100.00	100.00	100.00	100.00	100.00	100.00	100.00	100.00	100.00	100.00

[†]The "total" chemical composition of the dried, as-received biomass ash was calculated based on the XRF of each sieved fraction. For example, the wt.% Na_2O content of S1 was calculated according to: (0.61 wt.% x 67 wt.%) +(0.65 wt.% x 17 wt.%) + (1.37 wt.% x 16 wt.%) = 0.74 wt.%.

likelihood of devitrification, particularly if the glass is fed to the forming machine at relatively low temperatures or high viscosities during the manufacture of large articles[1]:

$$D = WRI - 160°C$$

where WRI = working range index, as defined above. Values of D vary; however, +15°C had become common in the global container glass industry by the year 2010.[1]

3 | RESULTS

3.1 | Sieving of biomass ash

The weight percentage of each ash fraction after sieving is given in Table 4.#ijag16637-fig-0002.fig The main particle size fraction is above 2000 μm, around 67 to 82 wt.%. The fraction of fine particles (≤63 μm) is close to that of the intermediate-sized particles (from 2000 to 63 μm) in S1 and

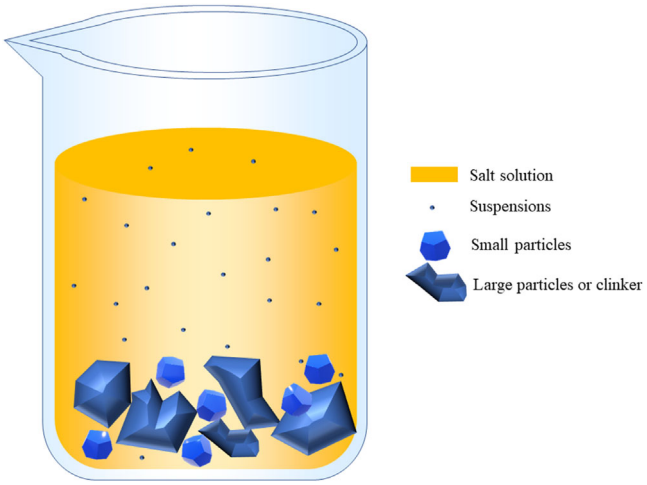

FIGURE 2 An illustration of the separation between ash particles of different sizes during water washing process.

S3. In S2, the weight percentage of the fine ash particles is two times larger than that of the intermediate fraction. The XRF results for each ash fraction are provided in Table 4. Carbon content was also characterized by LECO as it can impact the redox of the batch and glass produced using it.[55,56,64] The results are included in Table 4.

3.2 | Washing of biomass ash

Impurities such as Cl, S, and C could limit the application of biomass ash as glassmaking raw materials, therefore a further washing process was employed on selected biomass ash samples (S1) to investigate its effectiveness for Cl and S removal. After washing and filtration, the as-received ashes were separated into 3 parts (Figure 1): (i) salt evaporated from filtered solution; (ii) suspension or fine powders collected on the filter paper; (iii) small residue particles (0.5 to 3 mm in diameter) and large clinkers (>4 mm in diameter). The separation between ash particles of different sizes during the water-washing process was also illustrated in Figure 2. The weight percentage of each fraction after drying is listed in Table 5.

XRD was applied for the identification of any phase differences between those components after washing and filtration. XRD patterns for the as-received unwashed S1 sample are shown in Figure 3. The XRD patterns for the extracted salt, filter, and residue particles after washing are shown in Figure 4.

SEM and EDX characterizations were conducted on the as-received biomass ash (2000–63 μm) samples as shown in Figure 5. The SEM and EDX of the suspension/filtered fine powder from S1 biomass ash after washing and filtration are presented in Figure 6. As can be seen in Figure 7, the small particles (≈2 mm in diameter) present in the residue of the washed S1 sample have a smooth conchoidal surface. The SEM and EDX data of the S1 clinkers after washing and filtration processes are presented in Figure 8.

3.3 | Microstructural analysis on salt and insoluble residues from bracken ash after washing

Samples of bracken salt and insoluble residue for the simulation of ancient glass raw materials were characterized to compare with the biomass ash. The XRD patterns for bracken salt and residue are presented in Figure 9. The SEM and EDX of the bracken fine ash residue after the washing and filtration processes are presented in Figure 10. In Figure 11, a relatively large particle surface of bracken ash residue after washing and filtration was characterized with SEM and EDX.

3.4 | Melting of green soda-lime-silica container glass batches incorporating biomass ash

To highlight the impact of biomass ash on glass composition and properties, different amounts of treated biomass ash were directly added into representative green soda-lime-silica container glass batches[55,56] and melted under laboratory conditions. Each glass batch composition is shown in Table 1. Table 1A presents batch compositions in grams and Table 1B shows the batch compositions in weight percent. All treated biomass ashes were dried before batching. For glass batches 1–3 in Table 1B, 4.76 wt.% of washed biomass ash of different particle sizes was directly introduced into the benchmark glass batch without changing the levels of other ingredients. For glass batches 4–6, 4.76 wt.% sieved biomass ash was added. For glass batches 7–9, 9.09–16.67 wt.% of large particles (> 2 mm in diameter) of washed ash was added. For glass batches 10–12, 9.09–16.67 wt.% large particles (> 2 mm in diameter) of sieved ash were added. Accordingly, the normalized XRF results of each glass sample are also given in Table 2. The UV-Vis-Near IR absorption spectrum of each glass is shown in Figure 12. The baseline glass is shown in every group as the benchmark.

4 | DISCUSSION

4.1 | Sieving and washing of biomass ash

From Table 4, considerable alkali contents, especially potassium, are present in the ashes before and after

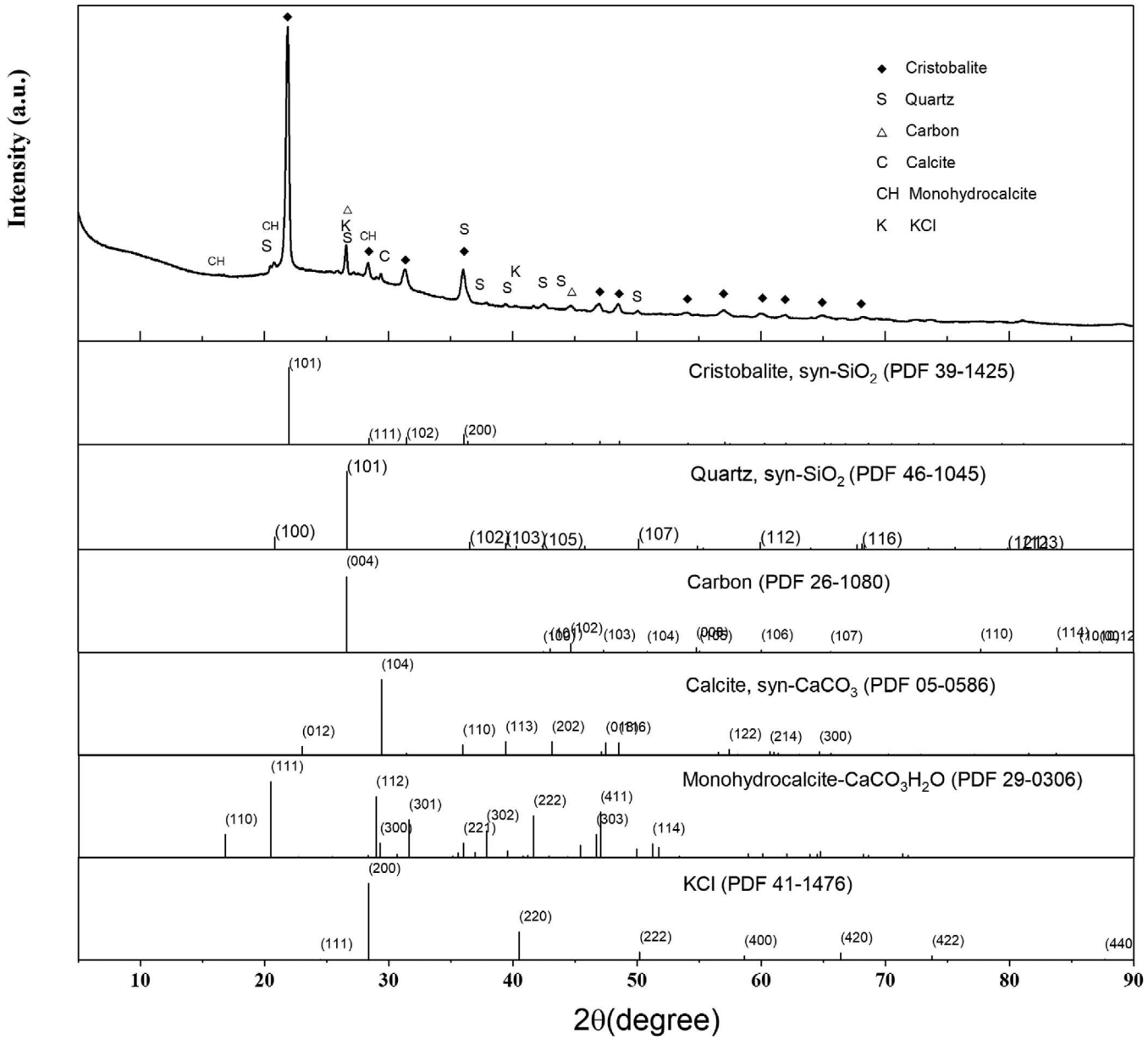

FIGURE 3 X-ray diffraction (XRD) patterns for the as-received S1 biomass ash and standard patterns for identified phases.

TABLE 5 Components of biomass ash after washing and filtration.

Dried biomass ash	DI water volume before washing	Solution volume after washing	Wt.% of salt from solution	Wt.% of suspended/fine particles	Wt.% of small particles and clinker
20 g	400 ml	340 ml	0.282	1.538	97.800

sieving. Alkaline earth metals Ca and Mg are in moderate abundance (around 10 wt.%) with a CaO: MgO ratio of around 4:1 (by weight). No Pb or other heavy metal elements were detected by XRF. The contents of transition metal ions such as Fe and Ti were minimal and the contents of other components such as Al were moderate. The analyzed K_2O contents of these ash fractions can be high, up to 26 wt.%, in the order S1 ≈ S2 < S3. The concentration of potassium in S1 increased with increasing particle size from 11.2 to 22.8 wt.% K_2O, which is similar to that of S3. However, the potassium distribution in S2 is decreased with increasing particle size, from 23.96 to 18.96 wt.% K_2O. The abundance of sodium is less than 1 wt.% Na_2O but the pattern of Na_2O distribution in all three biomass ashes

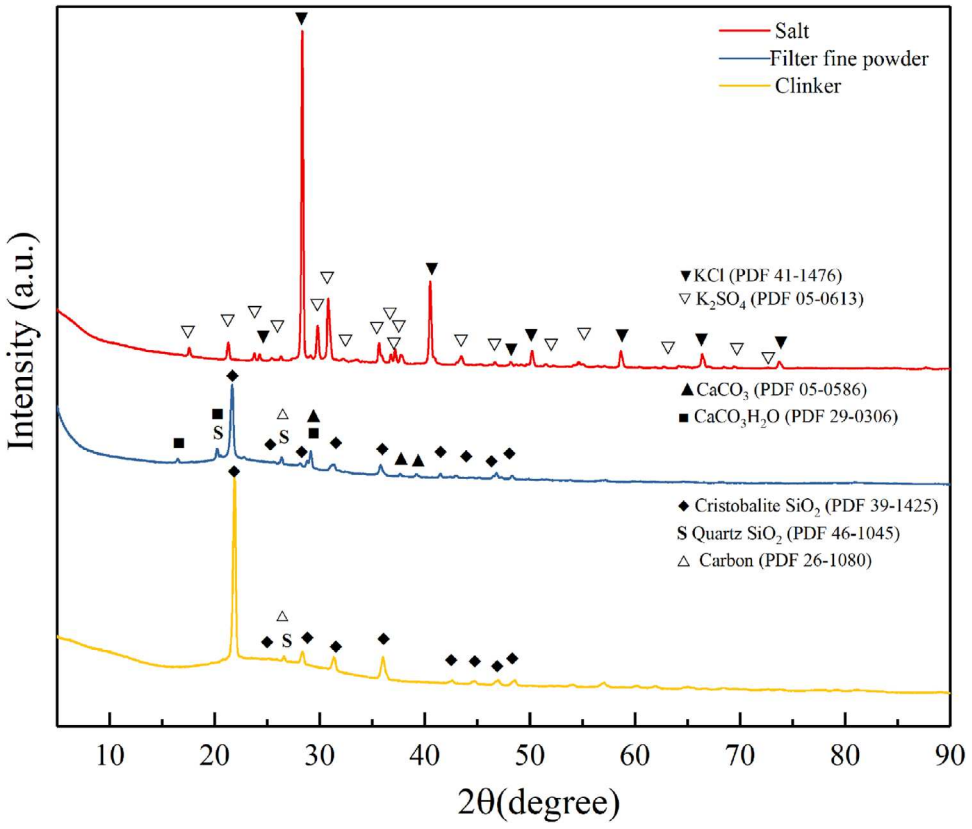

FIGURE 4 X-ray diffraction (XRD) patterns for the extracted salt, filter, and residue from S1 biomass ash after washing.

increased with decreasing particle size. The abundance of Cl is low in all three ash samples (≈0.35 wt.% in S1 and S2, and 0.56 wt.% in S3). Meanwhile, the concentration of Cl in all three ashes decreased with increasing particle size. Similar sulfur content decreased with increasing particle size for all three ashes. The lowest concentration of sulfur, ~0.15 wt.% SO_3, can be found in the > 2000 μm fraction of S2. The concentrations of phosphorus in all three ashes were relatively low (from 0.86 to 0.94 wt.% P_2O_5) without apparent fluctuation. The abundance of carbon follows the S1 < S2 < S3 trend similar to that of potassium. Meanwhile, carbon concentration in all three ashes decreased with increasing particle size. Furthermore, carbon concentration in fine particles (<63 μm) of S2 was high (up to 13.3 wt.%) which increased the total carbon content in the as-received S2 sample to 3.02 wt.%. Similarly, the carbon content in the < 63 μm fraction of S3 reached 26.05 wt.%. However, more encouragingly, the measured carbon content in the > 2000 μm fraction in all ashes was only 0.55 wt.%.

Generally, biomass ash compositions can be complex, in that the ashes contain mainly inorganic matter composed of different constituents, from amorphous compounds to crystalline phases and, additionally, organic matter composed of char and other organic materials.[19] The elements in those ashes can be separated into three groups, mostly present as compounds consisting of oxides, which include oxides of non-volatile elements such as Ca, Si, Mg, Fe, or Al; fluxes and volatile elements including K, Na, S, or Cl; and finally, heavy metal/volatile elements such as Zn, Cd, or Pb.[20] In Figure 13, the distribution of biomass ash particle size after sieving and the concentration of critical components, including K_2O, Cl, SO_3, P_2O_5, and C, based on XRF and LECO analyses are summarized. Similar trends in all three biomass ashes can be detected. All samples were dominated in mass by particles of > 2 mm in diameter. The concentration of K_2O in this particle group was relatively high compared to the other proportions whilst the concentrations of P_2O_5, SO_3, Cl, and C were relatively low. This demonstrates that a simple sieving process can, at least in some instances, effectively separate less desirable elements and compounds (as glass batch raw materials) from larger sized particles.

As shown in Table 5, the soluble salt content of S1 biomass ash was negligible and made up 0.282 wt.% of the total ash after washing and filtration, while the fine suspension made up 1.538 wt.%, and the main part of biomass ash (solid particles and clinkers) made up 97.8 wt.% of the total ash. Meanwhile, for the after-washed solution, the concentration of total salts, KCl and K_2SO_4, was approximately 141 mg/L, which is considerably lower than the reported limit

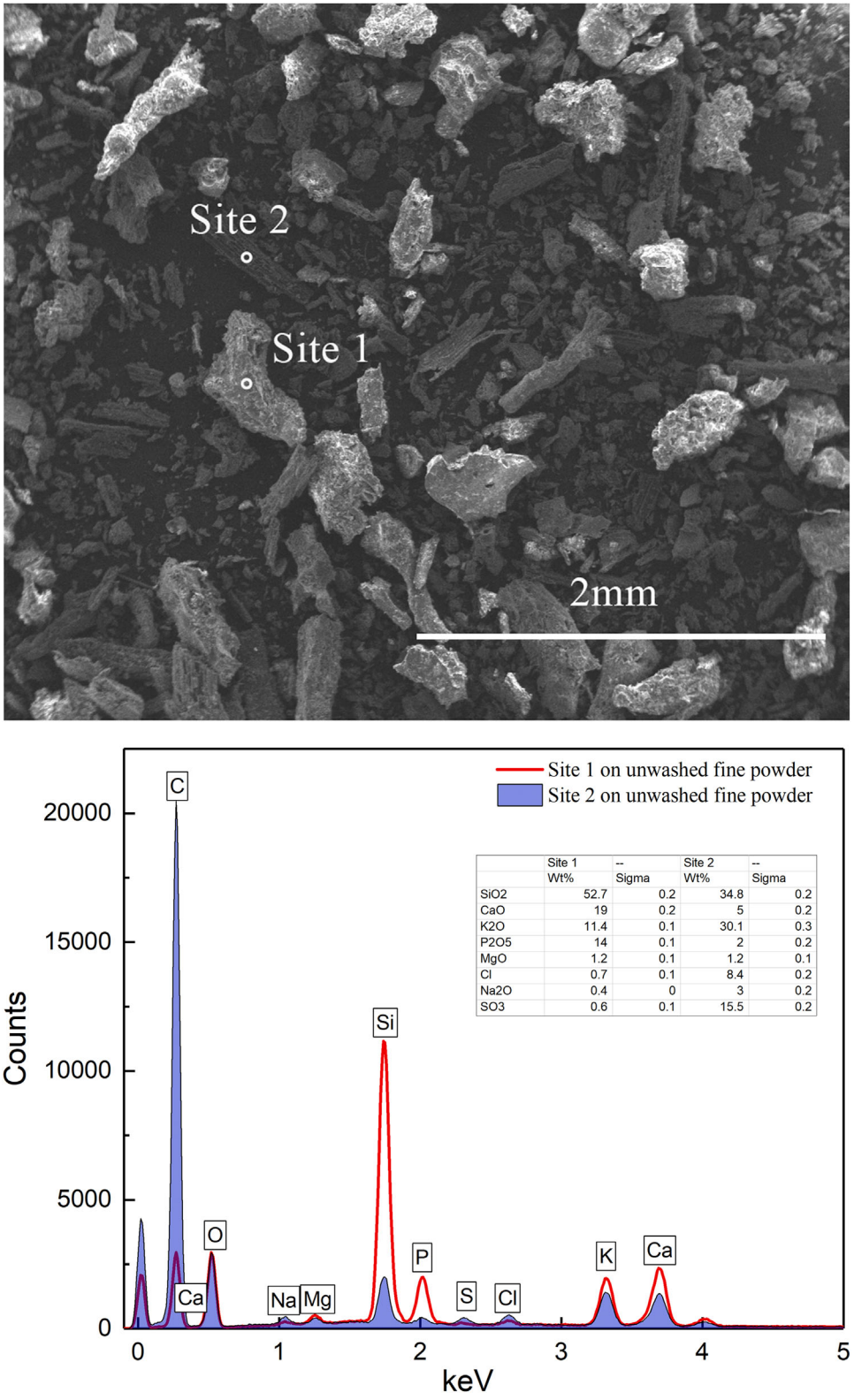

FIGURE 5 Secondary electrons (SE) SEM image of fine unwashed biomass ash S1 and EDX spectra of two different kinds of particles.

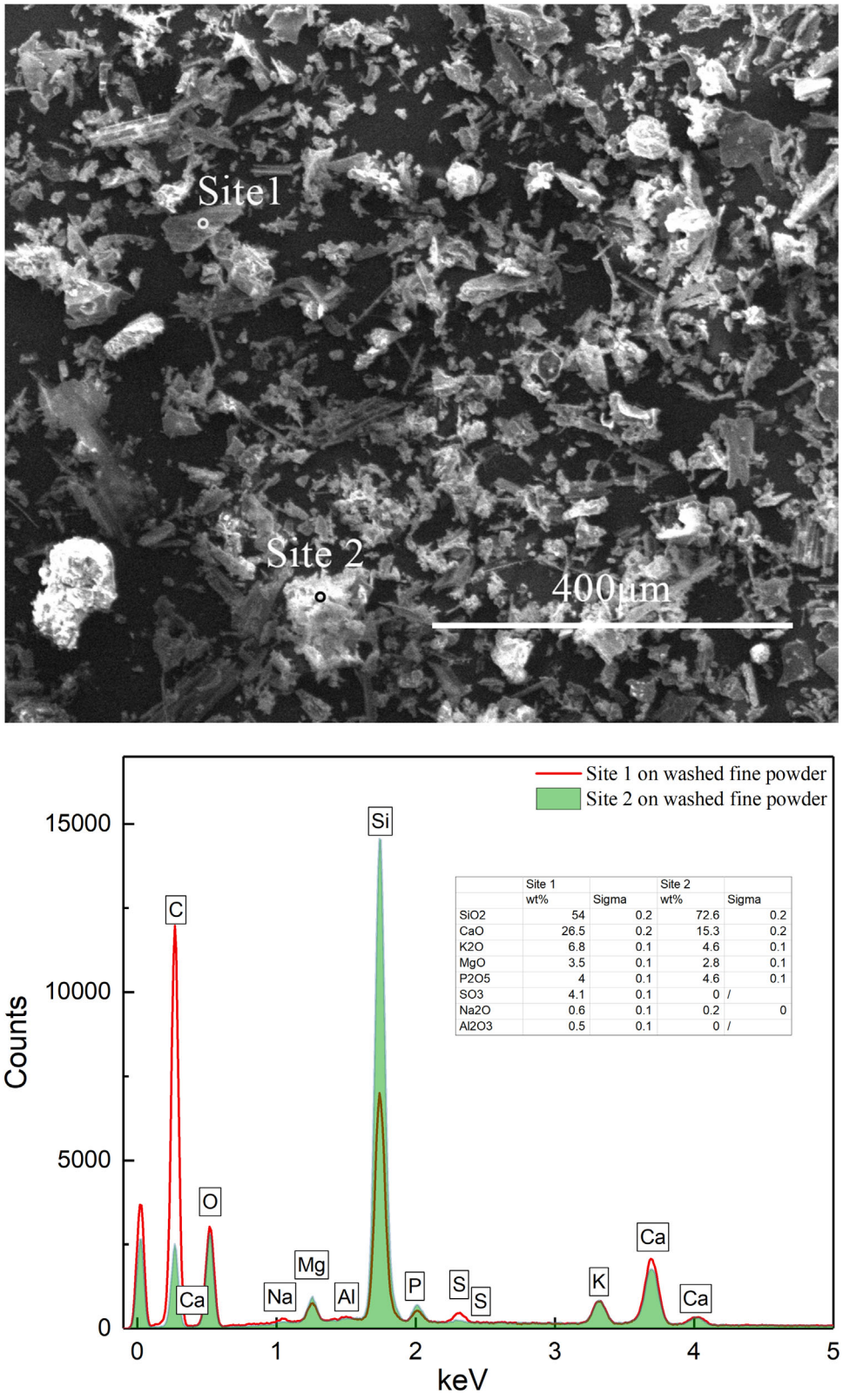

	Site 1		Site 2	
	wt%	Sigma	wt%	Sigma
SiO2	54	0.2	72.6	0.2
CaO	26.5	0.2	15.3	0.2
K2O	6.8	0.1	4.6	0.1
MgO	3.5	0.1	2.8	0.1
P2O5	4	0.1	4.6	0.1
SO3	4.1	0.1	0	/
Na2O	0.6	0.1	0.2	0
Al2O3	0.5	0.1	0	/

FIGURE 6 Secondary electrons (SE) SEM image of suspension/filtered fine powder from washed S1biomass ash and EDX spectra on two different kinds of particles.

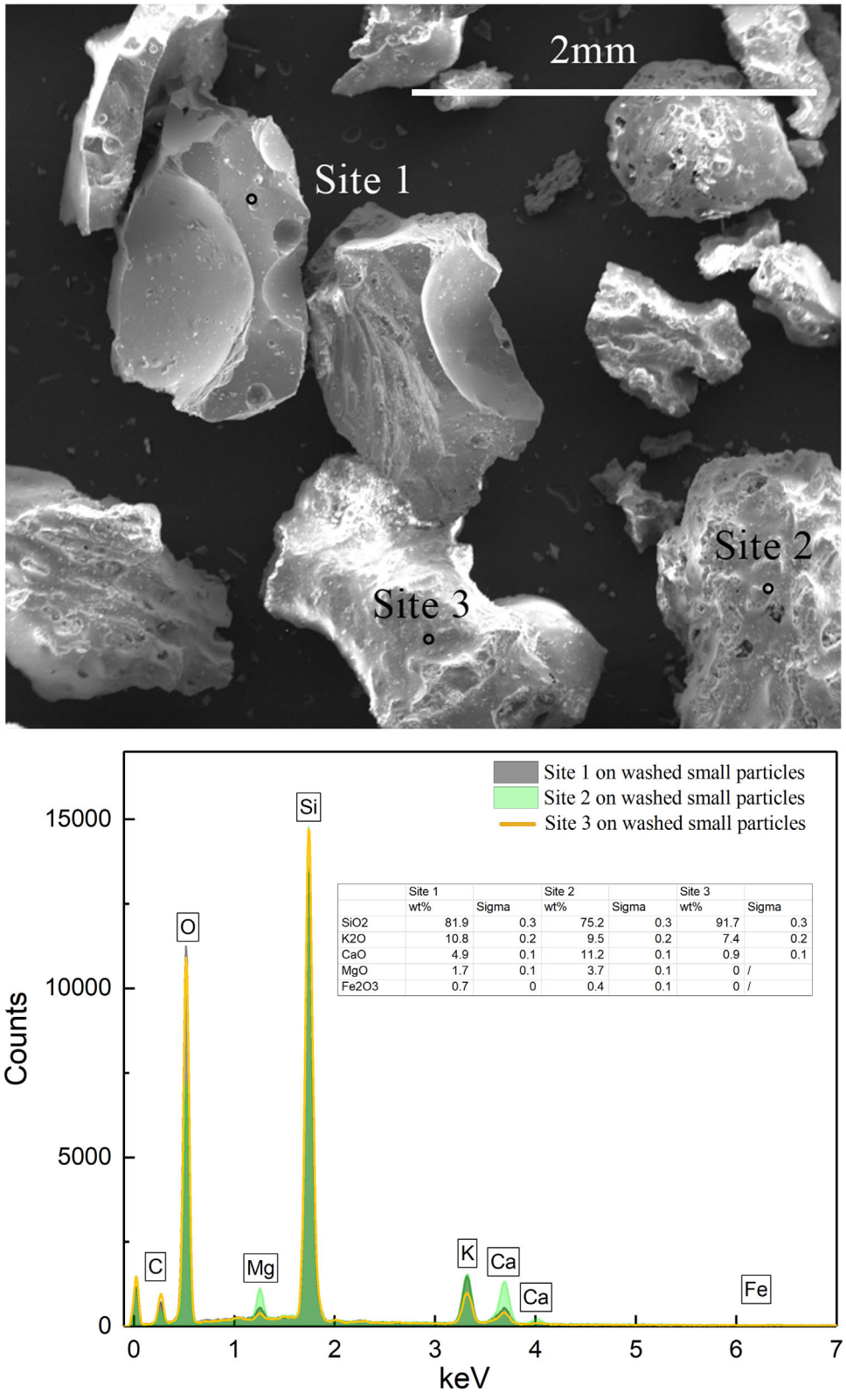

	Site 1		Site 2		Site 3	
	wt%	Sigma	wt%	Sigma	wt%	Sigma
SiO2	81.9	0.3	75.2	0.3	91.7	0.3
K2O	10.8	0.2	9.5	0.2	7.4	0.2
CaO	4.9	0.1	11.2	0.1	0.9	0.1
MgO	1.7	0.1	3.7	0.1	0	/
Fe2O3	0.7	0	0.4	0.1	0	/

FIGURE 7 Secondary electrons (SE)SEM image of small particles in the residue of washed S1 and EDX spectra on those particles.

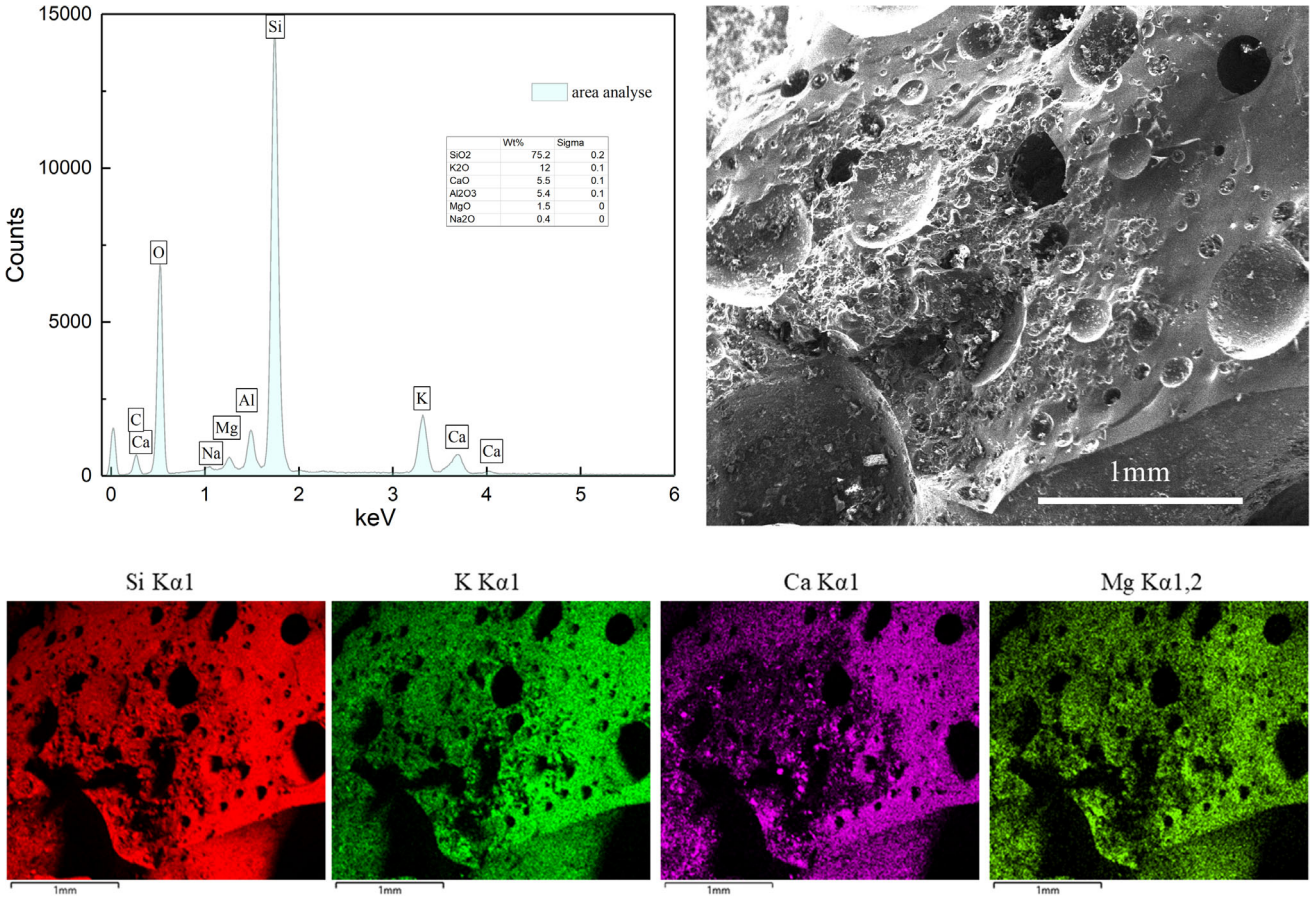

FIGURE 8 Secondary electrons (SE)SEM image of clinker surface in the residue of washed S1 and EDX mapping spectra and area analysis spectra on its surface.

for the monitoring of UK discharges to wastewater[66] (chloride is up to 1000 mg/L and sulfate is up to 5000 mg/L).

XRD patterns of un-washed S1 biomass ash are shown in Figure 3. Two main phases, Cristobalite and Quartz (SiO_2), were identified from the XRD analysis. A possible main phase, carbon, is presented here with its main diffraction peak (004) overlapping with the quartz (101) peak. Two minor phases, calcite ($CaCO_3$) and monohydrocalcite ($CaCO_3$ H_2O) were also identified. A possible minor phase, KCl, was identified. However, its main diffraction peak (200) overlaps with the (111) peak of cristobalite while other weak peaks such as (220) and (222) are challenging to discern considering the low levels of KCl, and the interference of other phase diffraction peaks. After identification, the main phases for S1 ash were determined to be cristobalite and quartz (SiO_2); a possible main phase may be carbon; and the minor phases may be $CaCO_3$, $CaCO_3{\cdot}H_2O$, and KCl.

XRD patterns for the extracted salt, filter, and residue particles after washing are presented in Figure 4. The extracted salt appeared as a white, deliquescent crystal powder which, according to the XRD analysis, is mainly composed of a KCl crystalline phase (PDF #41-1476) with a minor K_2SO_4 crystalline phase (PDF #05-0613). The crystalline phases in the filtrate or fine powders were determined to be cristobalite and quartz (SiO_2) with possible carbon, $CaCO_3$, and $CaCO_3{\cdot}H_2O$. The presence of an amorphous phase is also suggested by the weak "hump" centered around 28° 2θ. The amorphous hump is particularly evident in the XRD patterns for the large clinker particles. Cristobalite, quartz, and a possible trace amount of carbon can be identified. However, no $CaCO_3$ phase was identified.

SEM and EDX characterizations were conducted on the as-received S1 biomass ash and those three proportions after washing, shown in Figures 5–8. In Figure 5, two different kinds of particles can be observed in the unwashed biomass ash. A sharp-edged, platelike, or lath-like fragment is shown in the image at Site 2. Another type of particle has a more regular, less angular topography (Site 1). From the EDX data, the chemical compositions of those two different particles were not the same. Although the carbon coating does have a significant impact on the quantitative analysis of carbon, the EDX carbon difference is clearly apparent. This is consistent

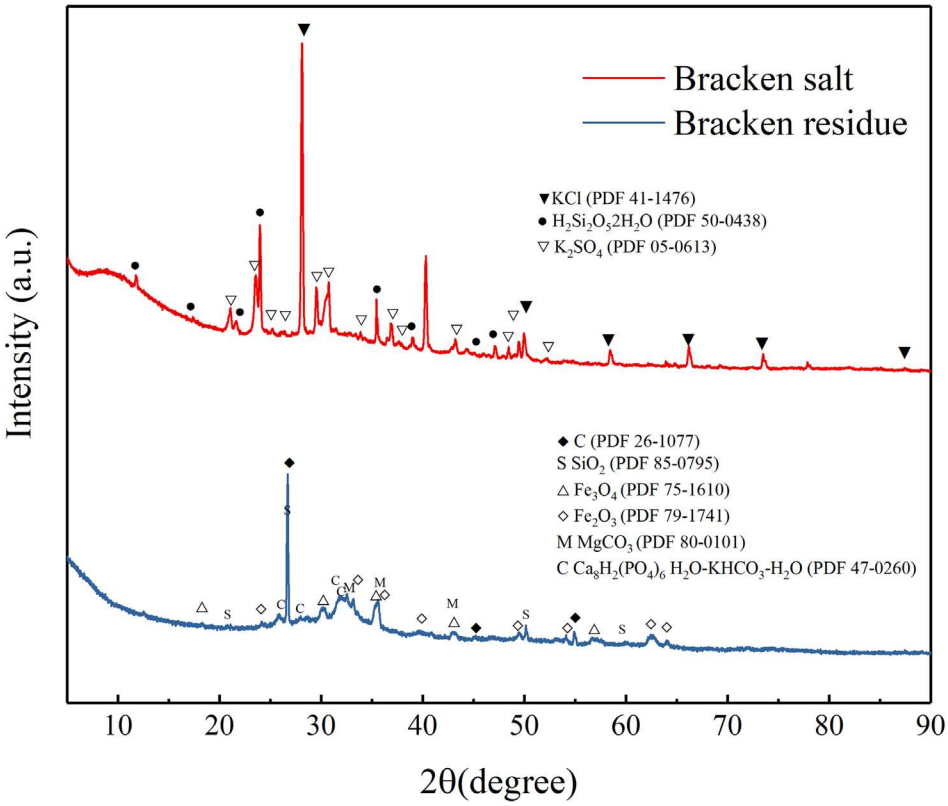

FIGURE 9 X-ray diffraction (XRD) patterns for bracken salt and insoluble residue.

with the carbon distinction in those two kinds of particles qualitatively. EDX analysis indicates that those platelike fragments are high in carbon and those more regular particles are high in silicon and phosphorus with low carbon content.

In Figure 6, The SEM and EDX on the suspension/filtered fine powder from S1biomass ash after washing and filtration are presented. Similarly, in the as-received biomass ash, two different particles, high carbon platelike fragments, and high silicon regular particles, were detected. The sizes of those particles were around 100 μm, which is much smaller than that of particles in the as-received biomass ash after sieving (63–2000 μm). From EDX, Cl is not determined in those suspensions.

As shown in Figure 7, small particles with diameters around 2 mm in the residue of washed S1 appear to have a smooth conchoidal surface. Based on EDX data, concentration of Cl in > 2000 μm particles fraction of S2 that made up the majority (72 wt.%) of the as-received ash is only 0.11 wt.%. The EDX data indicated that those particles were high in Si, Ca, and K, and low in carbon, while Cl and S were not detected. The consistency in the EDX data suggests that the compositions of those particles were similar and well-distributed.

The SEM and EDX on the surface of clinker from the S1 biomass ash residue after the washing and filtration process are presented in Figure 8. The morphology of clinker contained many bubbles and conchoidal fractures with different sizes, which suggests melting and liquid phase formation at high temperatures. Conchoidal fracture also suggests that those clinkers have mechanically fractured after the formation of the liquid phase. Therefore, the small particles that also contain bubbles and have conchoidal morphologies are likely to be the fragments of these clinkers after a fracture. Moreover, the XRD pattern for this material (Figure 4) clearly shows that the amorphous phase is a major component, evidenced by the characteristic broad amorphous "hump" centered at approximately 28°2θ. The EDX data shows that the distribution of essential elements such as Si, Ca, K, and Mg in those clinkers was uniform with no signs of other impurities such as C, S, and Cl.

4.2 | Bracken ash for ancient glass manufacture

For comparison, samples of bracken salt and insoluble residues for the simulation of ancient glass raw materials were also characterized. In Figure 9, the XRD patterns for bracken salt and residue are presented. Except for KCl (PDF #41-1476) and K_2SO_4 (PDF #05-0613), a crystalline

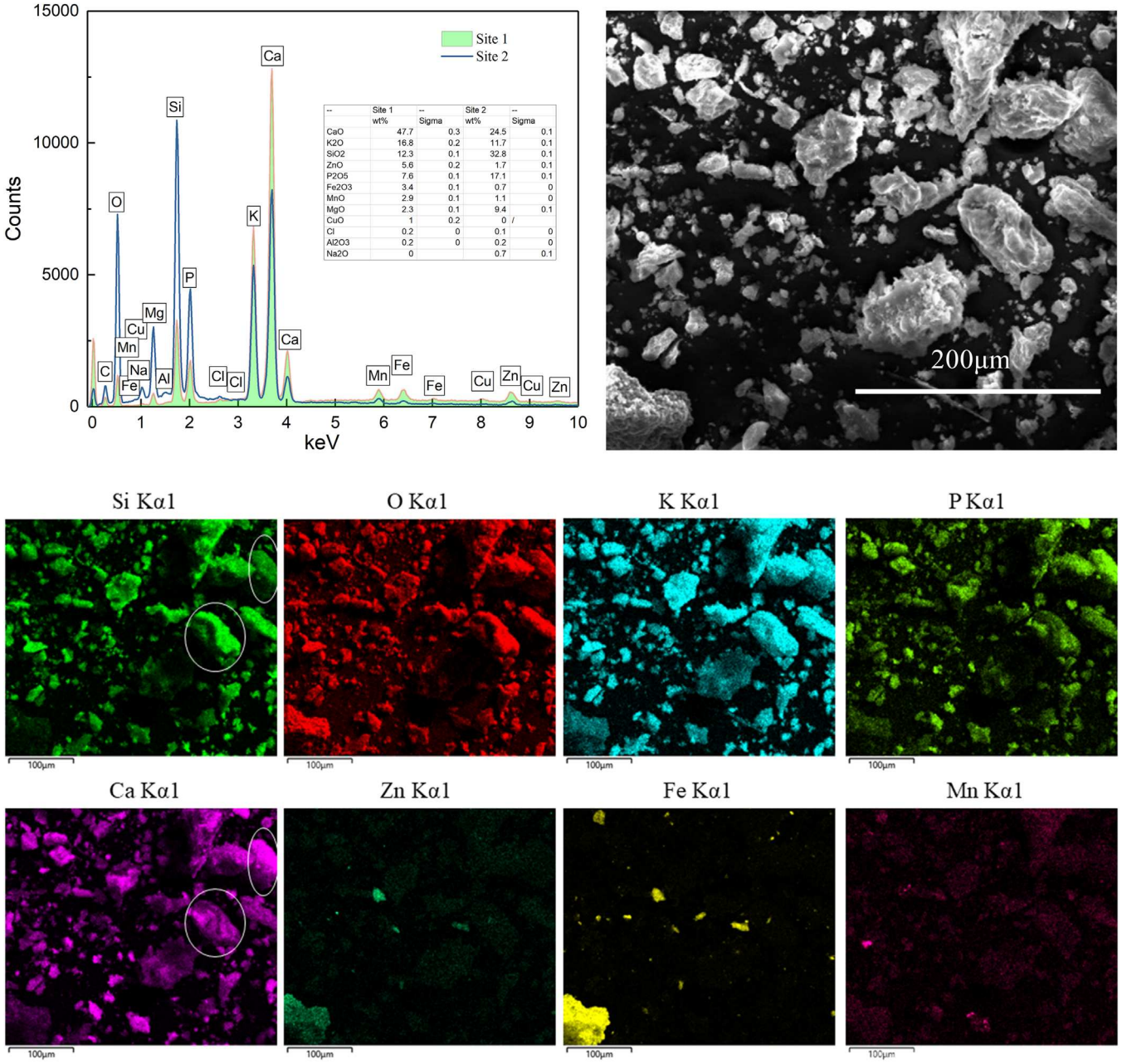

FIGURE 10 Secondary electrons (SE) SEM image of fine bracken residue and energy-dispersive X-ray (EDX) mapping spectra plus point spectra on particles.

silica gel phase (PDF #50-0438) was also determined in the salt, in addition to the amorphous phase confirmed by the "amorphous hump" in the diffraction pattern. The phases determined by XRD to be present in bracken ash insoluble residue are complex, including the main phases SiO_2 and carbon, and minor phases Fe_3O_4, Fe_2O_3, $MgCO_3$, and a complex calcium- and phosphorus-bearing phase.

The SEM and EDX on the bracken fine ash residue after the washing and filtration process are presented in Figure 10. The morphologies of those ashes are similar to each other. However, the chemical compositions are quite different. As observed from the EDX mapping analysis, the elemental distributions of Si, Ca, K, and P are not the same. Clusters or regions rich in metal elements including Fe, Zn, and Mn were also determined in mapping spectra. Two EDX spectra on different sites were also presented here for illustration. From the EDX spectrum, one site is rich in Ca, and the other is rich in Si, P, and O. Meanwhile, impurities including Fe, Zn, Mn, and Cl were identified.

In Figure 11, a relevant large particle surface of bracken ash residue after washing and filtration was characterized by SEM and EDX. Cracks and fragments can be observed

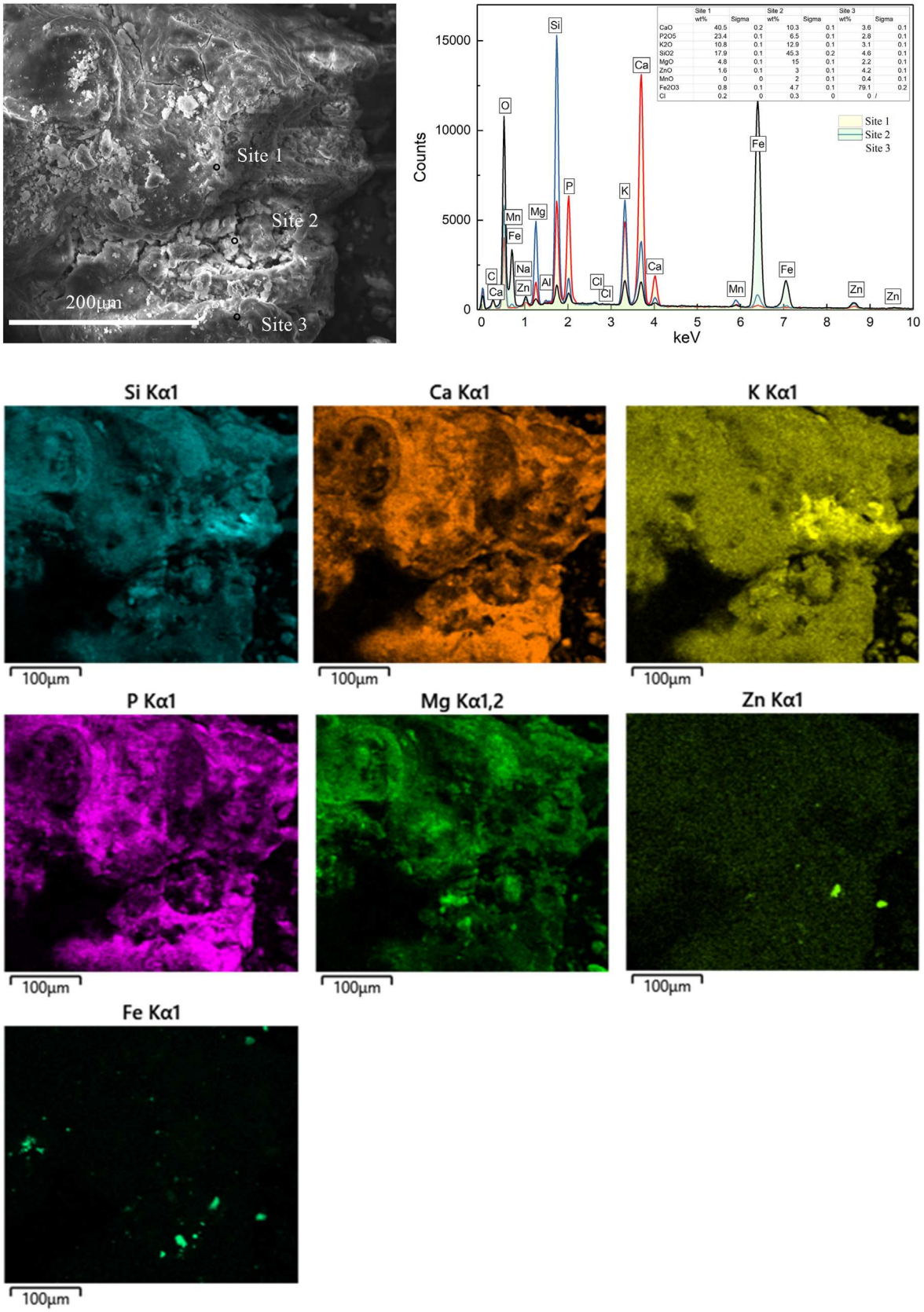

FIGURE 11 (SE) SEM image of a large particle in bracken residue and energy-dispersive X-ray (EDX) mapping spectra plus point spectra on its surface.

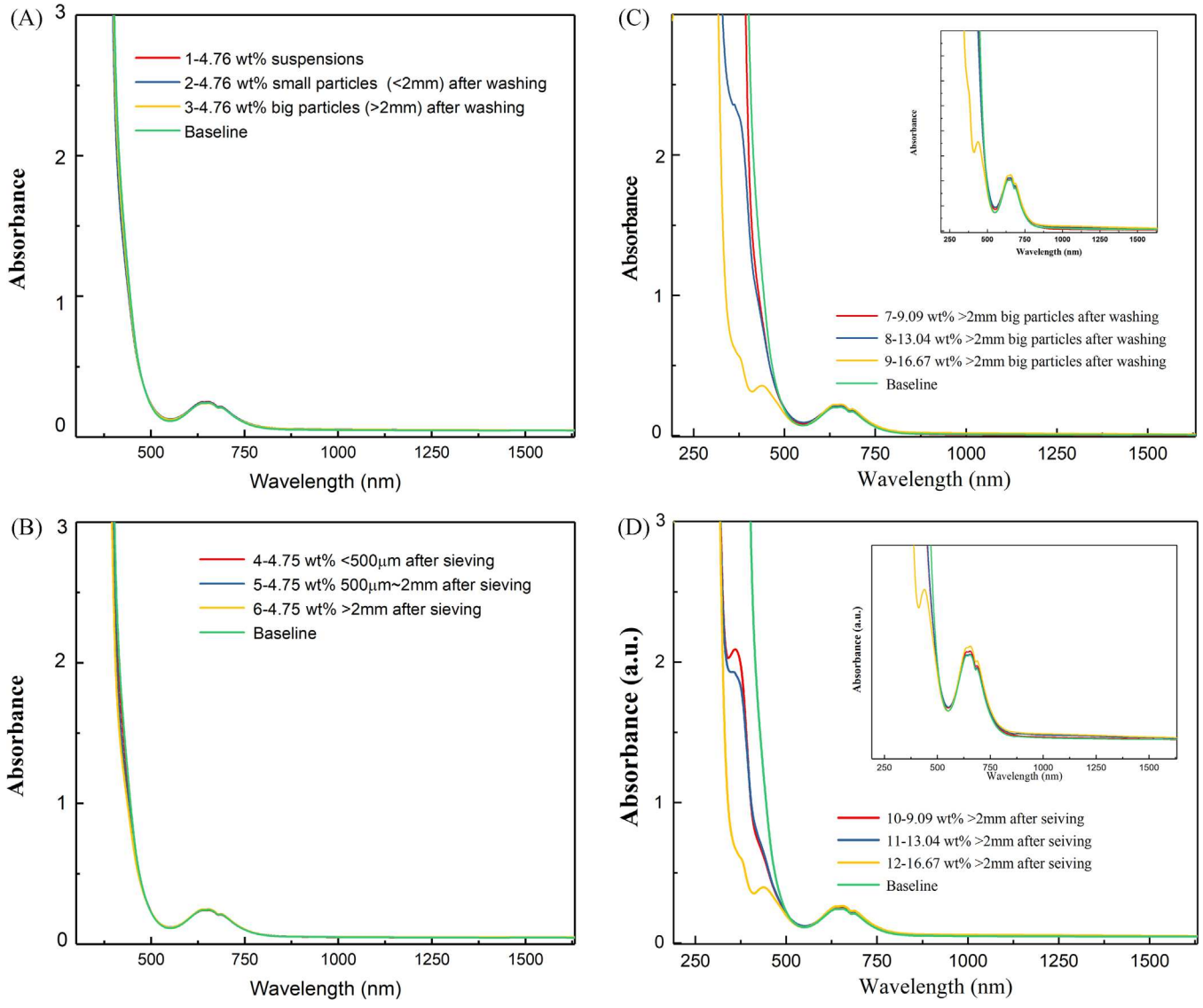

FIGURE 12 (A) Ultraviolet-visible near-infrared (UV-Vis-Near IR) absorption spectra of samples baseline, 1, 2, and 3. (B) UV-Vis-Near IR absorption spectra of samples baseline, 4, 5, and 6. (C) UV-Vis-Near IR absorption spectra of samples baseline, 7, 8, and 9. (D) UV-Vis-Near IR absorption spectra of samples baseline, 10, 11, and 12.

on the surface. The mapping EDX spectroscopy analysis suggests an uneven distribution of chemical elements on the surface. Clusters rich in metal elements, including Fe, Zn, and Mn, were determined again. From the quantitative EDX spectra, the chemical compositions of three sites on the surface of particles are quite different, one site is rich in Ca and P, one is rich in Si, K, Mg, and O, and one is rich in Fe. Meanwhile, impurities including Zn, Mn, and Cl were also determined.

It is interesting to note the difference between biomass ash and bracken insoluble residue in terms of their chemical compositions and elemental distributions. Many factors impact this since the plant for biomass fuel is quite different from the bracken. The plant species, place of origin, harvest season even part of the plant can all significantly affect the final ash composition.[42,54] Moreover, the combustion temperature of plant/biomass should also not be neglected. The morphology of clinker/residue in biomass ash indicates liquid phase formation leading to amorphous (glassy) formation upon cooling (confirmed by XRD). Modern industrial combustion processes give rise to high temperatures, sufficient to generate liquid phases which, if sufficiently rich in glass-formers such as SiO_2, form amorphous phases upon cooling. More volatile elements such as C, S, and Cl are also exhausted, and the ash composition was (relatively) purified. For ancient bracken ash, the lower combustion temperature and less detailed control did not purify those elements as effectively by comparison, as may reasonably be expected.

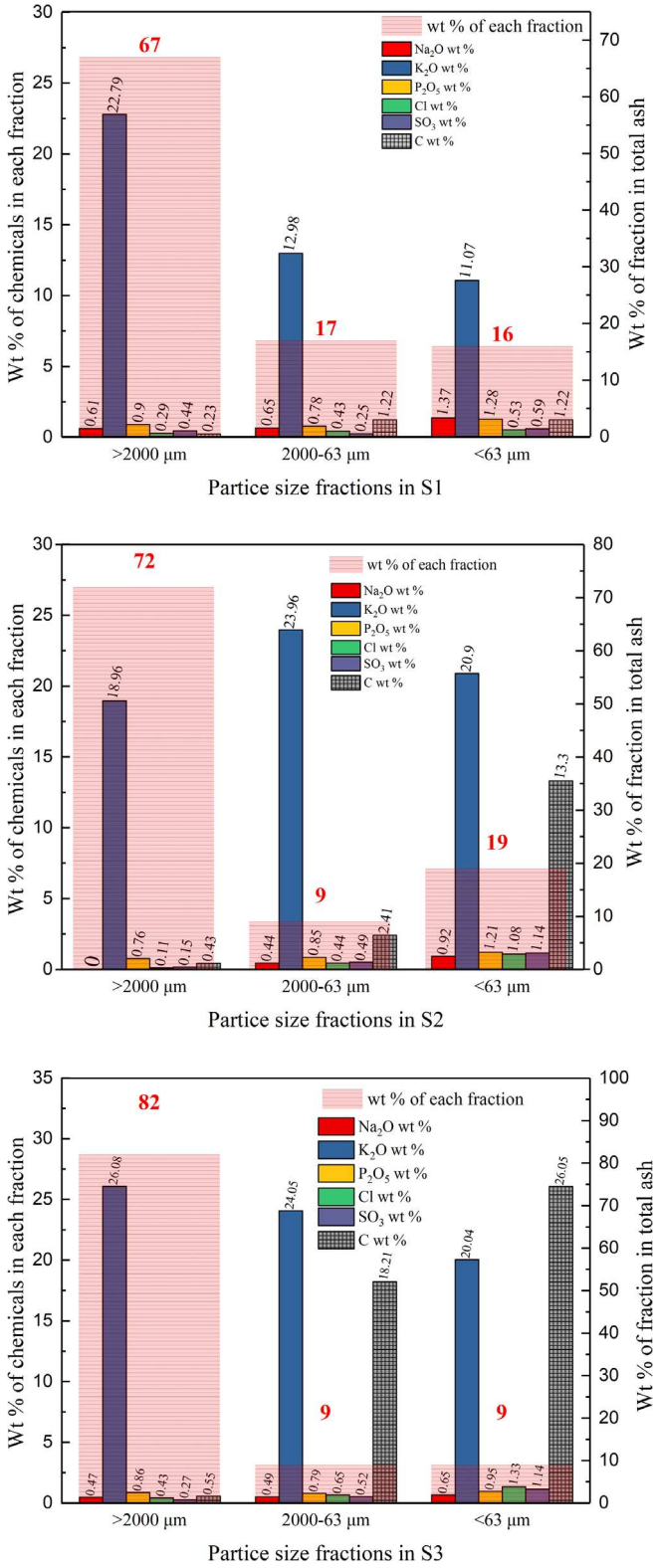

FIGURE 13 Biomass ash particle size distributions after sieving and critical element concentration distribution in each fraction (S1–S3).

4.3 | Biomass ash impact on green soda-lime-silica container glasses

The biomass ash is rich in SiO_2, and K_2O and contains notable CaO, P_2O_5, MgO, Al_2O_3, and Fe_2O_3 contents, as discussed above in Section 4.1. In Figure 14, the variations of those components in each glass were summarized to visualize biomass ash's impact on glass composition. The introduction of different types and amounts of biomass ash had little measured impact on the Cr_2O_3 and SO_3 contents of the glass: the former fluctuates around 0.3 wt.% and the latter fluctuates around 0.1 wt.%. Even when the added biomass ash was increased from 9.09 to 16.67 wt.% in glasses 7–12, this did not have a significant impact on the abundances of those two elements. Cl was hardly detected in those glass samples, and the highest amount in glass 12 is only 0.06 wt.%. For Fe_2O_3, its content fluctuated around 0.557 wt.% ± 0.018 from Benchmark to Glass 6 with 4.76 wt.% of biomass ash. In glasses 7–9, Fe_2O_3 content slightly increased from 0.577 to 0.645 wt.% as more biomass ash was introduced, from 9.09 to 16.67 wt.%. Similarly, in glasses 10–12, Fe_2O_3 slightly increased from 0.539 to 0.679 wt.% as biomass ash content in the batch increased from 9.09 to 16.67 wt.%.

The most significant variations that can be observed are in the K_2O and P_2O_5 contents of the glasses, and their trends are similar. Since there is no measured P_2O_5 in the benchmark glass and none is deliberately added to the benchmark glass batch, all P_2O_5 in glasses 1–12 arises from the biomass ash. An introduction of 4.76 wt.% biomass ash can increase average K_2O content by 0.534 ± 0.018 wt.% and P_2O_5 content by 0.076 ± 0.005 wt.% based on XRF analyses of glasses 1–6. The biomass ash content of the batch was increased from 9.09 to 16.67 wt.%, K_2O and P_2O_5 contents of the resulting glasses also increased, as indicated by the arrows in Figure 13. The changes in abundances of K_2O and P_2O_5 in the glass are remarkably linear when correlated with the biomass ash content of the batches. Meanwhile, sieving and washing of biomass ash did not show a significant impact on glass composition, based on XRF analyses of glasses 1–6. However, only 4.76 wt.% biomass ash was introduced into those batches, which may not be sufficient to clearly expose any impact within the uncertainties associated with the analytical techniques employed. The impact upon the glass of adding biomass ash to the batch is also reflected in the modeled viscosity and relevant properties of the glasses produced, using the compositions confirmed by the XRF analysis results. Generally, the introduction of biomass ash into the batch increased the melting temperature of the glass (TLog 2, the temperature corresponding to log (η / dPa•s) = 2) and the glass transition temperature (TLog 13, the temperature

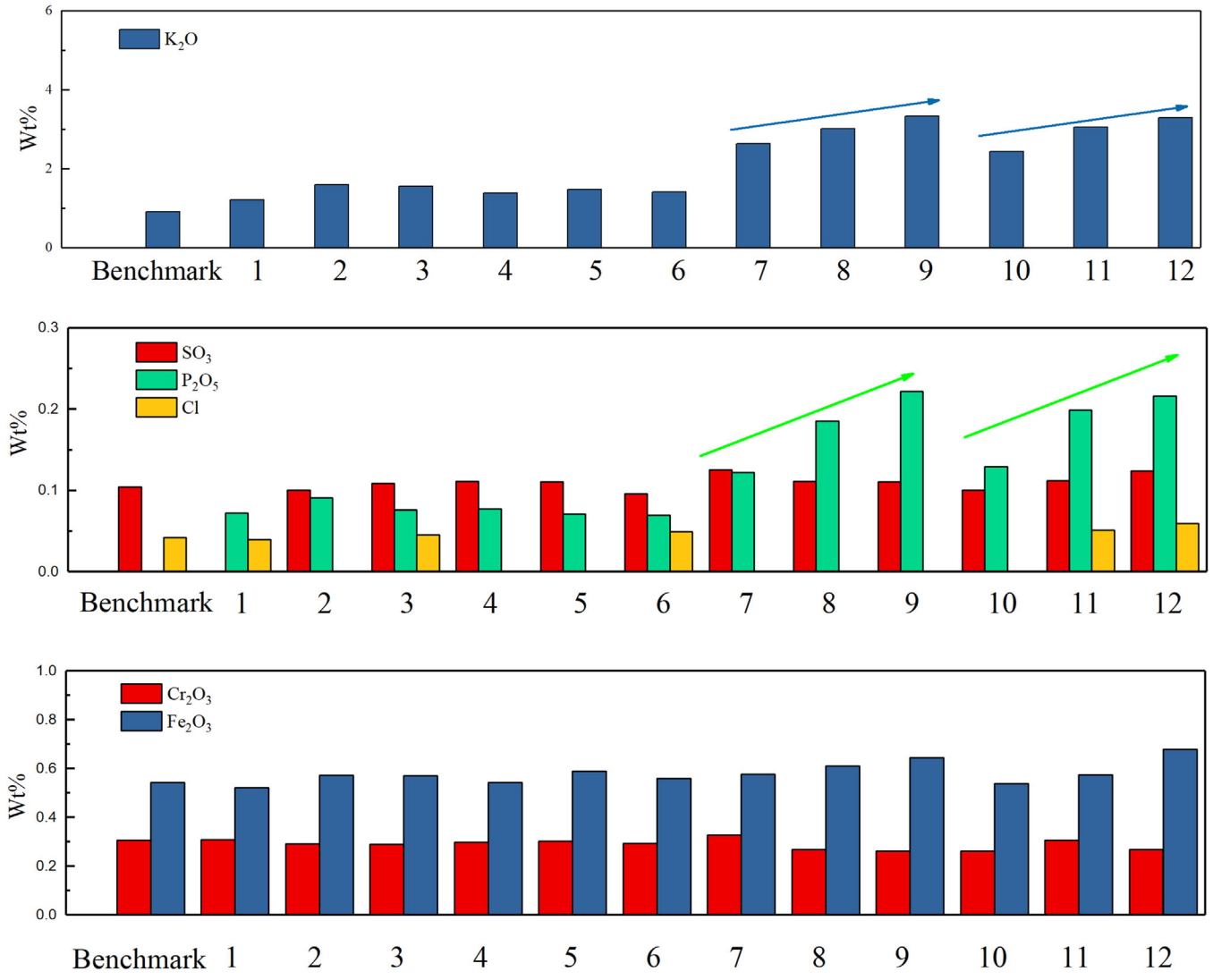

FIGURE 14 Variation of K_2O, SO_3, P_2O_5, Cl, Cr_2O_3, and Fe_2O_3 in each glass that biomass ashes were added in different proportions (arrows indicate a significant positive correlation between the abundance of elements K & P, and level of addition of biomass ash to the glass batch).

corresponding to log (η / dPa•s) = 13). Relative Machine Speed (RMS) did not change significantly, but the Devitrification Index was increased. It is important to note, however, that in this initial study, the biomass ash was simply added directly to the batch, with no compositional modification to accommodate it to the best advantage (for example with the aim of reducing TLog2), as would certainly need to be carried out before any future commercial implementation.[1,55,56,64,67]

Batch redox plays a vital role in glass manufacture, particularly in preparing homogeneous glass free from bubbles and making colored glasses containing transition metal ions.[1,55,56,64,68] To determine the impact of the different ashes on the glass properties as alternative raw materials, such as color, redox status, and transition metal ions status, UV-Vis-Near IR absorption spectroscopy was applied to all 13 glass samples to characterize the optical properties of the glasses in the near-UV, visible and near-IR regions and, thereby, the color and redox status. The UV-Vis-Near IR absorption spectra of the glasses are presented in four groups in Figure 12. The baseline glass is demonstrated in every group as the benchmark. For the spectra of the baseline glass, a distinctive absorption spectrum with a split, broad band centered at 660–700 nm is assigned to the $A_{2g}(F) \rightarrow {}^4E_{2g}(F)$ transition of Cr^{3+}.[55,56,64,68,69] In our previous research, the UV edge of green glass melted from a typical industrial glass batch is near 370 nm.[56] Interestingly, the UV absorption edge of the baseline green glass is up to ~500 nm. This is a sufficiently long wavelength to merge with the possible band occurring at ~450 nm due to the Cr^{3+} transition $A_{2g}(F) \rightarrow {}^4E_{1g}(F)$,[55,56,64,69] and a possible optical absorption

band centered at ~380 nm due to tetrahedrally coordinated Fe^{3+}, transition $^6A_1(S) \rightarrow {}^4E(D)$.[69,70] Meanwhile, no optical absorption band centered at ~1050 nm can be observed that would be assigned to the $^5A_2(S) \rightarrow {}^5E(D)$ transition of octahedrally coordinated Fe^{2+} cations.[69,70,71]

In Figure 12A, the spectra for green glass produced using 4.76 wt.% different washed biomass ashes are almost the same as that of the baseline, which indicates that the introduction of biomass ashes into the batch does not impact significantly the color and redox status of the glass. In Figure 12B, the spectra for green glass produced using 4.76 wt.% of sieved biomass ashes with different particle sizes are similar to that of the baseline. However, the UV edge occurs at around ~400 nm, which moves very slightly towards shorter wavelengths with increasing biomass ash particle size. In Figure 12C, as the batch content of the > 2 mm washed biomass ash increased from 9.09 to 16.67 wt.%, the UV edge moved to substantially lower wavelengths. For glass sample 7, the UV edge decreased to around 370 nm with the appearance of two shoulder bands, the band occurring at ~450 nm, attributable to the $A_{2g}(F) \rightarrow {}^4E_{1g}(F)$ transition of Cr^{3+},[55,56,64,69] and the band appearing at 360 nm attributed to a ligand to metal charge transfer (LMCT) band of Cr ions in Cr^{6+} oxidation state, which belongs to $^4A_{2g} \rightarrow {}^4A_{1g}$ transition.[71–74] As the ash increased up to 16.67 wt.%, the intensity of the band at ~360 nm continued to decrease, and the band at ~450 nm was fully revealed. A similar phenomenon can be observed in the spectra shown in Figure 12D for glasses with > 2 mm sieved as-received ash upon increasing from 9.09 to 16.67 wt.% biomass ash in the batch. Except for sample 12, a band centred at ~380 nm assigned to tetrahedrally coordinated Fe^{3+}, transition $^6A_1(S) \rightarrow {}^4E(D)$, and an abroad band centered at ~1050 nm assigned to the $^5A_2(S) \rightarrow {}^5E(D)$ transition of octahedrally coordinated Fe^{2+}, can be observed.[1,55,56,64,68–70]

For glasses, it is well known that glass redox status can be estimated through the redox couple of Fe^{2+}/Fe^{3+} or $Fe^{2+}/\Sigma Fe$ ratio.[1,56,64,68–71] As shown in the optical absorption spectra, another redox couple, Cr^{3+}/Cr^{6+} is also evidenced. According to the Lambert-Beer Law, the molar or specific extinction coefficient (or the transition probability) can reach a high value in fully-allowed charge transfer transitions.[74,75] A very intense charge transfer absorption band can be observed normally, nearby the intrinsic UV edge of silicate glass. Therefore, In the optical absorption spectrum of the benchmark glass, the very intense LMCT band of Cr^{6+} redshifts the UV edge and merges with the possible band of Cr^{3+} at ~450 nm and a possible absorption band of Fe^{3+}centred at ~380 nm.[74,76,77] The redox status of glass melted from laboratory reagents tends to be more oxidized than commercial glasses, partly because those chemicals contain less reducing impurities than that of industrial raw materials, and partly due to differences in furnace atmosphere and other factors.

As the biomass ash was introduced into the batch above 5 wt.%, the UV edge of the resulting glasses was blue-shifted, indicating a decrease in the intensity of the Cr^{6+} LMCT band. This indicates that more of the Cr^{6+} is reduced to Cr^{3+} in these glasses, due to the presence of higher levels of carbon in the batch, from the biomass ash. The equilibrium between chromium species in glass melt can be described by the following reaction[78]:

$$4CrO_3 \rightleftharpoons 2Cr_2O_3 + 3O_2$$

Since even low levels of Cr^{6+} can give rise to intense charge transfer bands, the amount of Cr^{6+} reduced to Cr^{3+} does not have a major impact on the *d-d* transition intensities of Cr^{3+} producing absorption bands at ~450 nm, as shown in Figure 12C,D. For the redox couple Fe^{2+}/Fe^{3+}, which is also sensitive to batch changes and redox conditions during melting, the absorption band of Fe^{3+} near 380 nm overlaps with the charge transfer band of Cr^{6+}. However, as the Cr^{6+} LMCT band decreases in intensity, this reveals the Fe^{3+} band more clearly. The absorption band attributed to Fe^{2+} at ~1050 nm can be only observed to increase noticeably in the spectrum for sample 12, produced using the highest biomass ash batch. This is consistent with the reduction of some Fe^{3+} to Fe^{2+}. As shown in the spectra for glasses 10 and 11, the major changes in the UV edge spectral region discussed above are consistent with oxidation of Cr^{6+} to Cr^{3+}, yet there was no significant change in the Fe^{2+} / Fe^{3+} ratio as evidenced by the lack of notable change in the Fe^{2+} band near 1050 nm. However, for glass 12, the UV edge continued to blue-shift and here the Fe^{2+} content increased as confirmed by the increase in intensity of the Fe^{2+} band near 1050 nm. Based on established redox potentials for soda-lime-silica glasses,[79] this suggests that all, or nearly all, of the Cr^{6+}, has preferentially been reduced to Cr^{3+} in glass 12, essentially eliminating the presence of Cr^{6+}, and the reducing melting conditions have thus also increased the Fe^{2+} / Fe^{3+} ratio as the next multivalent ion (Fe) available for redox change.[79]

As shown in Figure 12A,B, the addition of ~5 wt.% biomass ash to the glass batch had almost no impact on the color and redox status of the glasses produced here. This is attributed to the low carbon content and low levels of transition metal impurities in the biomass ashes, combined with their modest levels in the batch. From Figure 12C,D, it can be shown that ability to generate reducing glass melting conditions (due to carbon content) of the biomass ash after washing is lower than that of biomass ash after sieving, through observing the redox couple equilibrium of Cr^{3+}/Cr^{6+} by optical absorption spectroscopy.

5 | CONCLUSIONS

In this work, selected biomass ashes were treated by sieving and washing processes to decrease levels of undesirable impurities. XRF and LECO were applied on three batches of biomass ash after sieving, with 67 to 82 wt.% of ash particles being larger than 2000 μm. This largest size fraction contained the lowest carbon, chlorine, and sulfur contents, compared to the other, smaller, size fractions. The concentration of impurity elements increased with decreasing particle size, for example, carbon in S1 increased from 0.23 to 1.22 wt.% as the particle size decreased from more than 2000 μm to less than 63 μm. Considerable levels of alkali were concentrated in the > 2000 μm biomass ash size fraction. This indicates that sieving could be a simple and effective means to screen or optimize biomass ashes for use as, for example, alternative glassmaking raw materials. Water washing was applied to S1 biomass ash, with 0.28 wt.% of salt (KCl and K_2SO_4) washed from the ash. After washing, two different particle types, high carbon lath-like fragments, and more regular-shaped high-silicon particles, were detected in the suspension/filtered fine powder. Through EDX and SEM, the large particles of ash residue were observed to be in a vitrified state, confirmed by XRD and their morphologies. EDX mapping indicated that the chemical composition distribution is uniform and pure, rich in silicates, and very low in C, S, or Cl. Bracken salt and ash for ancient glass production were also characterized for comparison, the elemental distribution in the bracken ash being highly asymmetric and rich in impurities Fe, Zn, and Mn.

The morphology of the clinker/residue in biomass ash indicates liquid phase formation during the modern industry combustion process due to the high temperature. The volatile and flammable elements C, S, and Cl were also exhausted, and the ash composition was purified. For ancient bracken ash, the lower combustion temperature and unstable control cannot remove those elements as effectively by comparison.

UV-Vis-near IR absorption spectroscopy confirmed that 4.76 wt.% biomass ash additions to green soda-lime-silica container glass batches have little impact on the colour and redox state of the resulting glasses; and the ability of high levels of > 2 mm biomass ash additions to generate reducing glass melting conditions (directly related to carbon content) after washing is lower than that of biomass ash after sieving, as illustrated by changes in the redox couple equilibrium Cr^{3+}/Cr^{6+}.

ACKNOWLEDGMENTS

All authors acknowledge, with thanks, funding from Innovate UK (project EnviroAsh, reference # 49096). We acknowledge, with thanks, the biomass ash investigation and samples provided by Innovate UK-funded projects EnviroGlass 1, reference # 65839–429343 and EnviroGlass 2, reference # 8404, and the BEIS-funded project BiomAsh. WD and PAB also acknowledge, with thanks, funding from UKRI / EPSRC (TransFIRe Hub, EP/V054627/1). CMJ acknowledges and thanks NERC for funding (grant OSS/345/0507). All authors also thank the EnviroAsh project partners for useful discussions and practical knowledge gained from industrial-scale pilot trials delivered by Glass Technology Services Ltd.

ORCID

Wei Deng https://orcid.org/0000-0002-1793-8455
Paul A. Bingham https://orcid.org/0000-0001-6017-0798

REFERENCES

1. Wallenberger FT, Bingham PA. Fiberglass and glass technology: energy-friendly compositions and applications. New York: Springer; 2009.
2. UK Department for Business, Innovation & Skills and Department of Energy & Climate Change, Industrial Decarbonisation & Energy Efficiency Roadmaps to 2050: Cross Sector Summary. 2015. Available from: https://www.gov.uk/government/publications/industrial-decarbonization-and-energy-efficiency-roadmaps-to-2050
3. UK Department for Business, Innovation & Skills and Department of Energy & Climate Change. Industrial decarbonisation & energy efficiency roadmaps to 2050: glass. 2015. Available from: https://www.gov.uk/government/publications/industrial-decarbonization-and-energy-efficiency-roadmaps-to-2050
4. British Glass Manufacturers' Confederation. Glass sector net zero strategy 2050. Accessed March 04, 2023. Available from: https://www.britglass.org.uk/knowledge-base/resources-and-publications/glass-sector-net-zero-strategy-2050
5. Zier M, Stenzel P, Kotzur L, Stolten D. A review of decarbonization options for the glass industry. Energy Convers Manag X. 2021;10:100083.
6. Furszyfer Del Rio DD, Sovacool BK, Foley AM, Griffiths S, Bazilian M, Kim J, Rooney D. Decarbonizing the glass industry: A critical and systematic review of developments, sociotechnical systems and policy options. Renewable Sustainable Energy Rev. 2022;155:111885.
7. Glass futures' vision and mission. Accessed March 04, 2023. Available from: https://www.glass-futures.org/about
8. Mills J. Pilkington UK runs furnace on biofuel in four-day trial. 2022. Accessed March 04, 2023. Available from: https://www.glass-international.com/news/pilkington-uk-runs-furnace-on-biofuel-in-four-day-trial#:~:text=St%20Helens%20Councillor%20Mancyia%20Uddin,its%20furnace%20on%20100%25%20biofuel
9. Architectural glass production powered by hydrogen in world first. 2021. Accessed March 04, 2023. Available from:

https://www.nsg.com/en/media/ir-updates/announcements-2021/ag-production-powered-by-hydrogen
10. World's most sustainable glass bottles created in ground-breaking trial. 2021. Accessed March 04, 2023. Available from: https://www.glass-futures.org/worlds-most-sustainable-glass-bottles-created-in-ground-breaking-biofuel-trial
11. Morris G. Vidrala to install solar power installation at Spanish glass manufacturing facility. 2022. Accessed March 04, 2023. Available from: https://www.glass-international.com/news/vidrala-to-install-solar-power-installation-at-spanish-glass-manufacturing-facility
12. Morris G. Glass consortium aims to develop CO2-neutral container production. 2022. Accessed March 04, 2023. Available from: https://www.glass-international.com/news/glass-consortium-aims-to-develop-co2-neutral-container-production
13. Engie greens O-I Glass plants in Europe. 2022. Accessed March 04, 2023. Available from: https://renews.biz/76023/engie-greens-o-i-glass-plants-in-europe/
14. Allied Glass signs deal with Drax for 100% renewable hydropower. 2022. Accessed March 04, 2023. Available from: https://www.drax.com/uk/press_release/allied-glass-signs-deal-with-drax-for-100-renewable-hydro-power/
15. Transforming Foundation Industries Research and Innovation Hub. Accessed March 04, 2023. Available from: https://transfire-hub.org/
16. Transforming the Foundation Industries Network+. Accessed March 04, 2023. Available from: https://tfinetworkplus.org/
17. Ofgem, Biomass Sustainability Dataset 2019–20, London, Glasgow, Cardiff, 2021.
18. Tolivk consulting, UK Dedicated Biomass Statistics - 2017, Dursley, 2018.
19. Vassilev SV, Baxter D, Andersen L, Vassileva CG. An overview of the composition and application of biomass ash. Part 1. Phase–mineral and chemical composition and classification. Fuel. 2013;105:40–76.
20. Vassilev SV, Baxter D, Andersen L, Vassileva CG. Vassileva, An overview of the composition and application of biomass ash.: Part 2. Potential utilization, technological and ecological advantages and challenges. Fuel. 2013;105:19–39.
21. Rafieizonooz M, Mirza J, Salim MR, Hussin MW, Khankhaje E. Investigation of coal bottom ash and fly ash in concrete as replacement for sand and cement. Constr Build Mater. 2016;116:15–24.
22. Wang S, Terdkiatburana T, Tadé MO. Single and co-adsorption of heavy metals and humic acid on fly ash. Sep Purif Technol. 2008;58:353–8.
23. Sakhare VV, Ralegaonkar RV. Use of bio-briquette ash for the development of bricks. J Clean Prod. 2016;112:684–9.
24. Çiçek T, Çinçin Y. Use of fly ash in production of light-weight building bricks. Constr Build Mater. 2015;94:521–7.
25. Douglas RW, Frank S. A history of glassmaking. 1st ed. London and Tonbridge: The Whitefriars Press Ltd.; 1972.
26. Turner WES. Studies of ancient glass and glassmaking processes. Part I. Crucibles and melting temperatures employed in ancient Egypt at about 1370 BC. J Soc Glass Technol. 1954;38:436T–44T.
27. Turner WES. Studies of ancient glasses and glass-making processes. part ii. studies of ancient glasses and glass-making processes. J Soc Glass Technol. 1954;38:445T–56T.
28. Turner WES. Studies of ancient glasses and glass-making processes. part iii. the chronology of the glassmaking constituents. J Soc Glass Technol. 1956;40:39T–52T.
29. Turner WES. Studies of ancient glasses and glass-making processes. part iv. the chemical composition of ancient glasses. J Soc Glass Technol. 1956;40:162T–86T.
30. Turner WES. Studies in ancient glasses and glassmaking processes. Part V. Raw materials and melting processes. J Soc Glass Technol. 1956;40:277T–99T.
31. Tite MS, Shortland AJ. Production technology for copper- and cobalt-blue vitreous materials from the New Kingdom site of Amarna - a reappraisal. Archaeometry. 2003;45:285–312.
32. Tite MS, Bimson M. Glazed steatite: An investigation of the methods of glazing used in ancient Egypt. World Archaeol.. 1989;21:87–100.
33. Shortland A, Schachner L, Freestone I, Tite M. Natron as a flux in the early vitreous materials industry: sources, beginnings and reasons for decline. J Archaeol Sci. 2006;33:521–30.
34. Schlick-Nolte B, Werthmann R. Glass vessels from the burial of Nesikhons. J Glass Stud. 2003;45:11–34.
35. Phelps M, Freestone IC, Gorin-Rosen Y, Gratuze B. Natron glass production and supply in the late antique and early medieval Near East: The effect of the Byzantine-Islamic transition. J Archaeol Sci. 2016;75:57–71.
36. Jackson CM, Paynter S, Nenna MD, Degryse P. Glassmaking using natron from el-Barnugi (Egypt); Pliny and the Roman glass industry. Archaeol Anthropol Sci. 2018;10:1179–91.
37. Jackson CM, Cottam S. 'A green thought in a green shade'; Compositional and typological observations concerning the production of emerald green glass vessels in the 1st century A.D. Archaeol Anthropol Sci. 2015;61:139–48.
38. Freestone IC. Theophilus and the composition of medieval glass. MRS Proceedings. 1992;267:739–45.
39. Wedepohl KH. The change in composition of medieval glass types occurring in excavated fragments from Germany. Annales Du 14e AIHV Congres Venezia-Milano. AIHV Lochem; 1998/2000. pp. 252–7.
40. Kuisma-Kursula P, Räisänen J, Matiskainen H. Chemical analyses of European forest glass. J Glass Stud. 1997;39:57–68.
41. Welch CM. Glass-making in Wolseley, Staffordshire. Post-Mediev Archaeol. 1997;31:1–60.
42. Smedley JW, Jackson CM. Medieval and post-medieval glass technology: a review of bracken in glassmaking. Glass Technol. 2002;43:221–4.
43. Jackson CM, Smedley JW, Booth CA, Lane BC. Biringuccio on 16th Century Glassmaking. Lochem, the Netherlands; 2000:335–40.
44. Smith CS, Gnudi MT. The Pirotechnia of Vannuccio Biringuccio. New York: Dover; 1990.
45. McCray P. Glassmaking in Renaissance Venice. USA: Brookfield: Ashgate; 1999.
46. Brain C, Brain S. The development of lead-crystal glass in London and Dublin 1672–1682: a reappraisal. Glass Technol: Eur J Glass Sci Technol A. 2016;57:37–52.
47. King J. Specification of the Patent granted to Mr James King, of Newcastle upon Tyne, Merchant; for the new invented British Barilla. 1780.
48. Hopkins S. Patent X1: the making of Pot ash and Pearl ash by a new Apparatus and Process, 1790.

49. Barker TC, Dickinson R, Hardie DWF. The origins of the synthetic alkali industry in Britain. Economica. 1956;23:158–71.
50. Backhouse D, Guilbot A, Scrimshire A, Eales J, Wei D, Bell A, et al. Biomass ashes as potential raw materials for mineral wool manufacture: initial studies of glass structure and chemistry. Glass Technol: Eur J Glass Sci Technol A. 2022;63:19–32.
51. Kemp V, McDonald A, Brock F, Shortland AJ. LA-ICP-MS analysis of late bronze age blue glass beads from Gurob, Egypt. Archaeometry. 2020;62:42–53.
52. Shortland AJ, Tite MS. Raw materials of glass from amarna and implications for the origins of Egyptian glass. Archaeometry. 2000;42:141–51.
53. Deng W, Backhouse D, Kabir F, Janani R, Bigharaz M, Wardlow A, et al. An ancient technology could help deliver decarbonization. Glass Int. 2019;42:47–9.
54. Smedley JW, Jackson CM. Medieval and post-medieval glass technology: Bracken as a sustainable source of alkali? Glass Technol: Eur J Glass Sci Technol A. 2006;47:39–47.
55. Deng W, Wright R, Boden-Hook C, Bingham PA. Melting behavior of waste glass cullet briquettes in soda-lime-silica container glass batch. Int J Appl Glass Sci. 2019;10:125–37.
56. Deng W, Wright R, Boden-Hook C, Bingham PA. Briquetting of waste glass cullet fine particles for energy-saving glass manufacture. Glass Technol: Eur J Glass Sci Technol A. 2018;59:81–91.
57. UK Department for Environment Food & Rural Affairs, Area of crops grown for bioenergy in England and the UK: 2008–2020. Section 2: Plant biomass: miscanthus, short rotation coppice and straw. 2021. Available from: https://www.gov.uk/government/statistics/area-of-crops-grown-for-bioenergy-in-england-and-the-uk-2008-2020/section-2-plant-biomass-miscanthus-short-rotation-coppice-and-straw
58. Zhai J, Burke IT, Stewart DI. Beneficial management of biomass combustion ashes. Renewable Sustainable Energy Rev. 2021;151:111555.
59. Hartwell R, Coult G, Overend M. Mapping the flat glass value-chain: a material flow analysis and energy balance of UK production. Glass Struct Eng. 2022.
60. Griffin PW, Hammond GP, McKenna RC. Industrial energy use and decarbonization in the glass sector: A UK perspective. Adv Appl Energy. 2021;3:100037.
61. Jackson CM, Smedley JW. Medieval and post-medieval glass technology: seasonal changes in the composition of bracken ashes from different habitats through a growing season. Glass Technol Eur J Glass Sci Technol A. 2008;49:240–5.
62. Bell A, Backhouse D, Deng W, Eales J, Kilinc E, Love K, et al. X-ray fluorescence analysis of feldspars and silicate glass: effects of melting time on fused bead consistency and volatilisation. Minerals. 2020;10:442.
63. Lakatos T, Johansson LG, Simmingskold B. Viscosity temperature relations in the glass system SiO_2-Al_2O_3-Na_2O-K_2O-CaO-MgO in the composition range of technical glasses. Glass Technol. 1972;13:88–95.
64. Deng W, Spathi C, Coulbeck T, Erhan K, Backhouse D, Marshall M, et al. Exploratory research in alternative raw material sources and reformulation for industrial soda-lime-silica glass batches. Int J Appl Glass Sci. 2020;11:340–56.
65. Zhernovaya NF, Onishchuk VI, Kurnikov VA, Zhernovoi FE. Rapid evaluation of the workability of container glass. Glass Ceram. 2001;58:329–31.
66. UK Environment Agency. M18: Monitoring of discharges to water and sewer. 2017. Available from: https://assets.publishing.service.gov.uk/government/uploads/system/uploads/attachment_data/file/646803/LIT_6898.pdf
67. Bingham PA, Marshall M. Reformulation of container glasses for environmental benefit through lower melting temperatures. Glass Technol: Eur J Glass Sci Technol A. 2005;46:11–9.
68. Paul A. Chemistry of glasses. 2nd ed. London: Chapman & Hall; 1990.
69. Bingham PA, Connelly AJ, Hand RJ, Hyatt NC, Northrup PA, Alonso MR, et al. A multi-spectroscopic investigation of sulphur speciation in silicate glasses and slags. Glass Technol: Eur J Glass Sci Technol A. 2010;51:63–80.
70. Volotinen T, Parker J, Bingham P. Concentrations and site partitioning of Fe^{2+} and Fe^{3+} ions in a Soda–Lime–Silica glass obtained by optical absorbance spectroscopy. Glass Technol: Eur J Glass Sci Technol B. 2008;49:258–70.
71. Wright AC, Clarke SJ, Howard CK, Bingham PA, Forder SD, Holland D, et al. The environment of Fe^{2+}/Fe^{3+} cations in a soda–lime–silica glass. Phys Chem Glasses: Eur J Glass Sci Technol B. 2014;55:243–52.
72. Singh V, Chakradhar RPS, Rao JL, Kwak HY. Characterization, EPR and photoluminescence studies of $LiAl_5O_8$: Cr phosphors. Solid State Sci. 2009;11:870–4.
73. Sugawara T, Komatsu R, Satoshi U. Linear and nonlinear optical properties of lithium tetraborate. Solid State Commun. 1998;107:233–7.
74. Hassan MA, Ebrahim FM, Moustafa MG, El-Fattah ZMA, El-Okr MM. Unraveling the hidden Urbach edge and Cr^{6+} optical transitions in borate glasses. J Non Cryst Solids. 2019;515:157–64.
75. Möncke D, Ehrt D. Charge transfer transitions in glasses - Attempt of a systematic review. Opt Mater: X. 2021;12:100092.
76. Rao BL, Babu Y, Prasad S. Magnetic and spectroscopic properties of PbO-La_2O_3-P_2O_5:Cr_2O_3 glass system. J Non Cryst Solids. 2013;382:99–104.
77. Kesavulu CR, Chakradhar RPS, Jayasankar CK, Rao JL. EPR, optical, photoluminescence studies of Cr^{3+} ions in Li_2O-Cs_2O-B_2O_3 glasses - an evidence of mixed alkali effect. J Mol Struct. 2010;975:93–9.
78. Guloyan YA. Kinetics of chromium oxide transformations in glass melting. Glass Ceram. 2005;62:231–4.
79. Schreiber HD, Wilk Jr NR, Schreiber CW. A comprehensive electromotive force series of redox couples in soda–lime–silicate glass. J Non Cryst Solids. 1999;253:68–75.

How to cite this article: Deng W, Backhouse DJ, Kabir Kazi F, Janani R, Holcroft C, Magallanes M, et al. Alternative raw material research for decarbonization of UK glass manufacture. Int J Appl Glass Sci. 2023;1–25. https://doi.org/10.1111/ijag.16637